Abstract

Retrofitting of Unreinforced Masonry Walls
Using Fiber Reinforced Polymer Laminates

Khalid M. Mosalam and Reid R. Senescu

The report compares the structural response of unretrofitted unreinforced masonry (URM) walls with URM walls retrofitted on one side with glass fiber reinforced polymer (FRP) laminates. Six walls are experimentally investigated using the diagonal tension standard test procedure. In this investigation, two objectives are considered. First, a comparison is made between the improvements in performance provided by retrofitting a single-wythe wall versus that provided by retrofitting a triple-wythe wall. Second, the performance enhancement provided by the FRP is compared with two mortar-to-brick strength ratios. Various material tests are also performed to better analyze the experimental results.

The results from the tests are then compared with current standards for evaluating the design strength of URM walls. The strength enhancement provided by the FRP in the experiments is also compared with current standards for estimating the design strength contribution of FRP. In addition to these standards, the authors propose another alternative for estimating FRP design strength based on shear strain in the FRP.

The research shows that the application of FRP on only one side of a three-wythe wall prevents brittle catastrophic failure and may potentially improve the in-plane seismic response of a URM wall. Variability in test results, the small number of specimens tested, and the inability of the diagonal tension test to model real URM wall behavior limit the overall comparisons that can be made between the experimental results and the design standards considered.

TABLE OF CONTENTS

LIST OF FIGURES

LIST OF TABLES

ACKNOWLEDGEMENTS

Special thanks to Professor Stephen A. Mahin and Professor George C. Johnson for reviewing this report.

The staff at the Structures Laboratory at the University of California, Berkeley deserves our thanks for their help. In particular, the experiment portion of this research benefited considerably from the advice and diligent work of Lev Stepanov. We also appreciated the help of Professor Claudia P. Ostertag and graduate student Caroline Tsang. The diligent work and unwavering dedication of undergraduate student Evelyn Liang was also immensely appreciated. Also, the walls on which this research was based would not have existed without the bricklaying skills and voluntary work of several Berkeley students to which we are very grateful.

This research was supported by Sika Corporation and Lotus General Contractors, Inc. We appreciate the assistance provided by these companies as well as the technical guidance provided by Hexcel Corporation and Simpson, Gumpertz, & Heger Inc. We also would like to thank the National Science Foundation and the University of California, Berkeley for their support.

This material is based upon work supported under a National Science Foundation Graduate Research Fellowship. Any opinions, findings, conclusions or recommendations expressed in this publication are those of the authors and do not necessarily reflect the views of the National Science Foundation.

1 INTRODUCTION

1.1 Background

Observations from previous earthquakes show that buildings that depend on unreinforced masonry (URM) walls to resist seismic forces often experience severe damage relative to structures with other lateral resisting systems. Since damage to masonry buildings usually results in the falling of bricks, masonry buildings pose a serious life-safety threat even if complete structural collapse does not occur. Furthermore, masonry structures are a prevalent form of construction in the United States, constituting approximately 70% of existing buildings in 2001 (Tumialan, 2001). Though most of these structures exist east of the Rocky Mountains, a large number were built in the earthquake prone region along the West Coast prior to the consideration of seismic forces.

Because of the prevalence of URM, the development of appropriate retrofitting techniques is an important component of the effort to mitigate the disastrous effects of earthquakes on urban areas. Masonry structures generally depend on structural walls to resist lateral forces. If the shear forces caused by the inertia of upper floors are too great, the shear capacity of structural walls can be exceeded and the wall can fail in-plane. This type of failure is evident by the diagonal shear cracks in Figure 1.

Frequently, walls are weakened by window or door openings and failures occur in the piers between such openings. In-plane failures may also occur where low axial loads exist and the shear strength of bed joints is reduced. When axial load is low, failure may

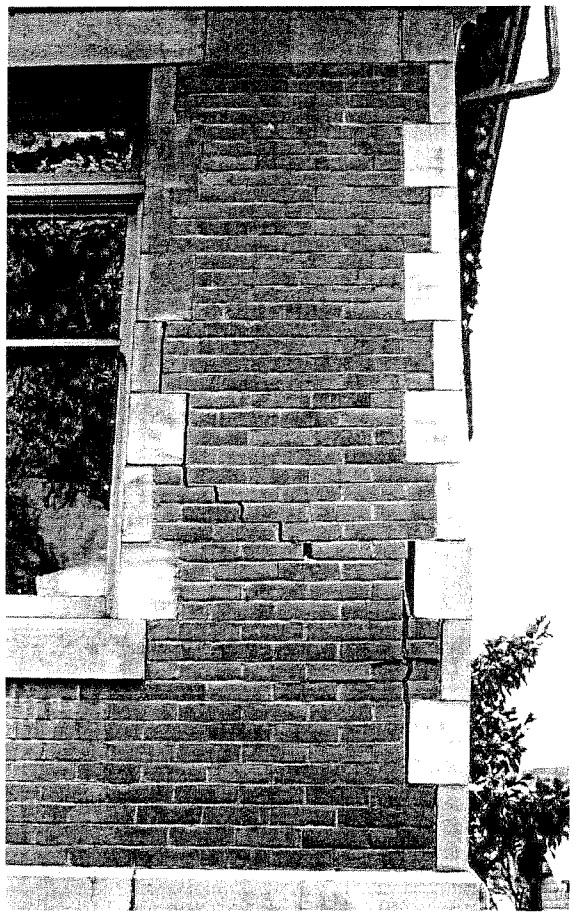

(a) Diagonal shear cracking in a corner pier next to a window in a URM building.

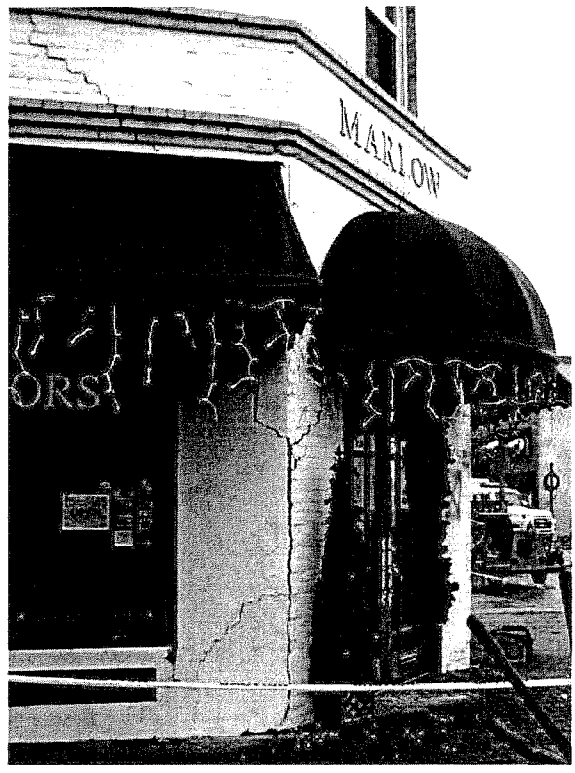

(b) Diagonal shear cracking throughout a URM building.

Figure 1: Observations from December 22, 2003 San Simeon, California earthquake (http://peer.berkeley.edu/san_simeonEQ/).

consist of either sliding of one entire wall section over another along the bed joint, or rocking action where the bed joint fractures and the top of the wall rocks on the bottom section. In-plane failure is generally the least severe mode of failure in URM structures since the wall can usually withstand gravity loads even after significant in-plane lateral strength is lost. However, in-plane failure generally allows excessive deflection of diaphragms, which can initiate other more catastrophic failure modes. Figure 2 shows a photograph of a URM building built in 1892 in Paso Robles, California, which experienced collapse of the second story during the 2003 San Simeon earthquake. The

Figure 2: Part of a URM wall section that is still standing despite the collapse of the rest of the second story. December 22, 2003 San Simeon, California earthquake (http://peer.berkeley.edu/san_simeonEQ/).

collapsed portion of the second story wall simply slid over the diagonal cracks leaving a small portion of the second story wall still standing. The similarly constructed buildings in Figure 1 also experienced in-plane cracking in the San Simeon earthquake, but the strength reduction caused by the cracks was not large enough to allow collapse.

URM is also frequently used to infill concrete frames. The URM contributes significantly to the lateral stiffness of the structure. Collapse of the infill causes significant threat to life and may allow the concrete frame to drift to potentially unstable displacements. An example of URM infill failure is shown in Figure 3.

The weakness of URM structures has long been recognized. In fact, as a result of severe damage to URM structures during the Long Beach, California earthquake of 1933, the use of masonry was temporarily prohibited in all public buildings in the state of California (Tumialan, 2001). In the 1940's and 1950's, masonry construction continued in

Figure 3: Reinforced concrete frame with collapse of brick infill and arched windows, August 17, 1999 Izmit (Kocaeli), Turkey earthquake (http://nisee.berkeley.edu/images/servlet/EqiisListQuake).

California in compliance with the Uniform Building Code, which required the design of masonry structures to withstand small seismic forces. Vertical steel reinforcement was used to resist the tensile forces that developed in the wall as a result of ground motion.

In 1981, Division 88 of the City of Los Angeles Building Code required that most URM buildings in Los Angeles undergo retrofitting (Kehoe, 1996). The ordinance required that URM parapets be removed or braced; that mortar joints be tested and walls strengthened to meet minimum values for shear strength; that walls meet certain clear height/thickness requirements; that walls be anchored to floor and roof diaphragms; and that diaphragms meet certain strength and stiffness requirements. It is important to recognize that this procedure was not intended to bring older buildings up to the design standards of current construction. Also, the goal of the provision was to ensure life-safety and not to limit economic losses.

As a result of increased consciousness of the potential effects of future earthquakes, much effort has been put forth to retrofit all types of structures in the Western United States over the last decade. Recently, fiber reinforced polymer (FRP) laminates have become popular for both concrete and masonry retrofits. Oftentimes, URM structures are historically significant, requiring minimal changes to exterior architectural appearance. Consequently, engineers often have limited access to the structural elements that require strengthening. Numerous tests have been conducted to evaluate the effectiveness of FRP as a retrofitting material. Previous research has used FRP on both sides of the wall or on one side of a single-wythe wall. In practice, historical structures typically have multi-wythe walls supporting gravity and seismic forces and frequently, engineers have access to only the interior side of the wall. This reality prompted the investigation of three-wythe URM walls retrofitted on one side with FRP.

1.2 Objective and Scope

The objective of the experiments conducted in this study is to evaluate the effectiveness of FRP in enhancing strength and ductility when applied to only one side of a three-wythe unreinforced masonry wall. In this study, two variables are investigated. First, a comparison is made between the improvements in performance provided by retrofitting a single-wythe wall versus that provided by retrofitting a triple-wythe wall. Second, the performance enhancement provided by the FRP is compared with two mortar-to-brick strength ratios. One pair of control and retrofitted specimens is tested with Type N (*weak*) mortar, and one pair of triple-wythe specimens is tested with Type M (*strong*) mortar. The same type of brick is used for all the walls. The test matrix in Table 1 shows the performed wall tests.

Table 1: Test matrix

Wall No.	Wythes	Mortar	Retrofit
1	1	N, Weak	None
2	1	N, Weak	FRP
3	3	N, Weak	None
4	3	N, Weak	FRP
5	3	M, Strong	None
6	3	M, Strong	FRP

A diagonal tension test slightly modified from ASTM E 519 was chosen, because of its similarity to the in situ stress state that would exist in a panel of bricks in a URM wall (ASTM, 1988). To simplify the test setup, a panel 30 in. by 30 in. was tested as opposed to the 48 in. by 48 in. panels recommended by the ASTM guidelines. The panels represent a prototype middle section of either a URM wall with shear and axial load forces or an infill wall bounded by a concrete frame with a compression strut forming along the diagonal. The URM and infill conditions are shown in Figure 4 (a) and (b), respectively. Regardless of the prototype chosen, a combined compression and shear force exists at the center of the panel, as shown in Figure 4 (c). To model this stress state, the wall panel is compressed in-plane across the diagonal using the test setup shown in Figure 4 (d). This setup creates the shear stress state shown in Figure 4 (e), which induces the diagonal tension cracking typically observed in prototype buildings. The San Simeon earthquake caused such a pattern of diagonal tension cracking in a URM wall shown in Figure 5, which appears very similar to the cracked test specimens to be discussed later with reference to Figure 16.

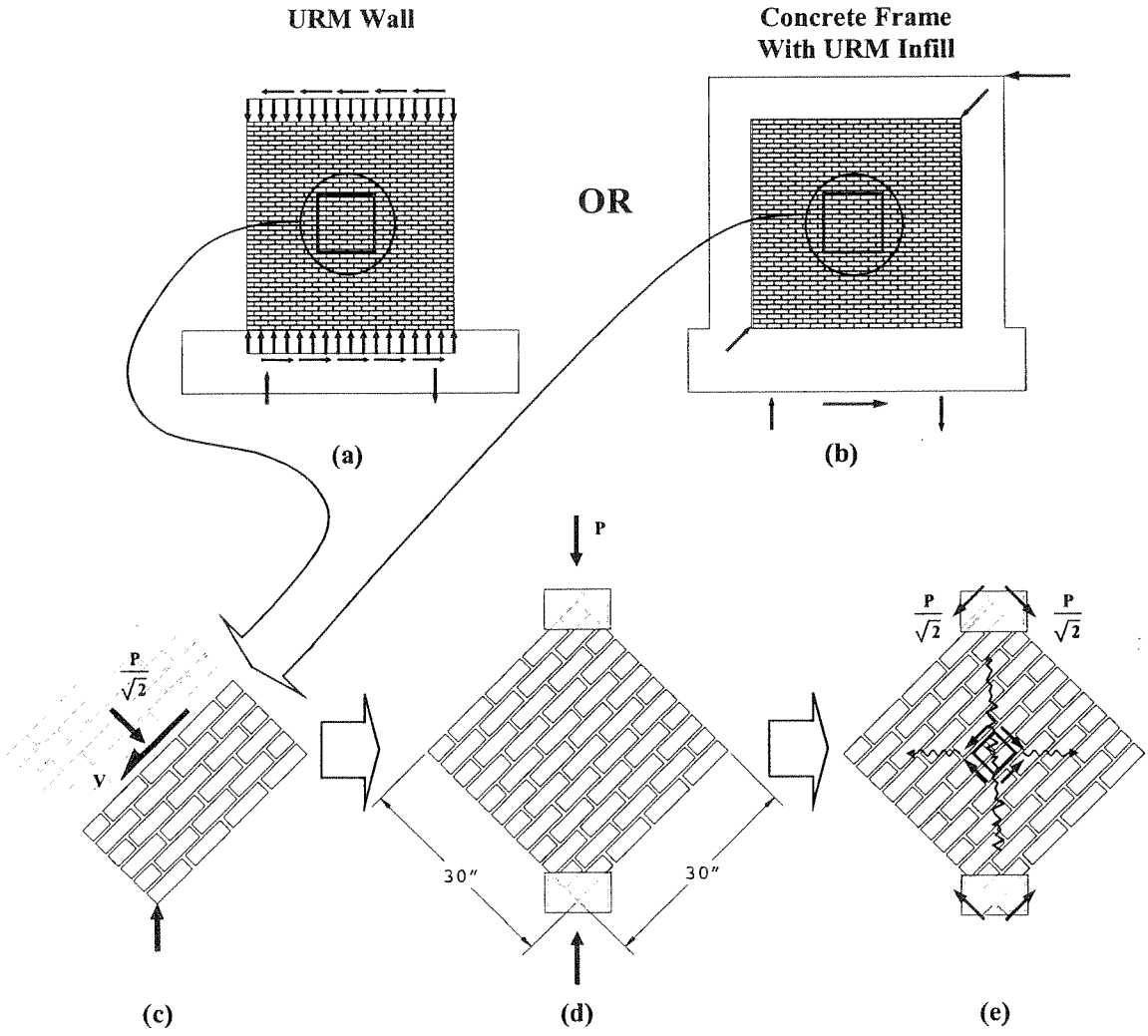

Figure 4: (a) URM wall. (b) Concrete frame with URM infill. (c) Equivalent free body diagram of the brick panel in the URM wall or URM infill prototypes. (d) Test setup. (e) Stress conditions at the center of the tested panel that induce vertical tension cracking.

Figure 5: A typical historic URM building with in-plane shear cracking in a multi-wythe load bearing wall. December 22, 2003 San Simeon, California earthquake (http://peer.berkeley.edu/san_simeonEQ/).

2 MATERIALS

Masonry is a complex composite of bricks and mortar. The behavior of a masonry wall depends on the properties of the brick units, the mortar, and the mortar-brick interface. Several tests of materials used in the construction of the panels were conducted to better understand the wall panel behavior. The materials, tests used to evaluate materials, and material test results are described in this section. After each test is discussed, photos and diagrams of several of the tests are shown in Figure 7 and Figure 8, and Table 7 lists average results for each material test as well as a coefficient of variation (COV).[1] The COV should be analyzed with caution since only a limited number of specimens were tested for each experiment.

2.1 Bricks

Clay bricks of dimensions 3-5/8 x 2-1/4 x 7-5/8 in. were provided by a local distributor. The bricks were manufactured by H.C. Muddox of Sacramento. They are Modular Brick Veneer units of color Dusty Rose that meet ASTM C 216, Grade SW, FBS for "Facing Brick" (ASTM, 2001). The bricks are cored with 2 rows of 5 holes of diameter approximately ¾ in. such that the net area is 85% of the gross area. A photograph of the type of brick used is shown in Figure 6. H.C. Muddox provided a data sheet written by American Testing Services Inc. on October 30th, 2000. Table 2 shows the

[1] The COV is based on the *biased* or n method of calculating the standard deviation. It assumes the entire population is sampled and calculates the COV using the equation, $COV = \frac{1}{\bar{x}}\sqrt{\frac{n\left(\sum x^2\right)-\left(\sum x\right)^2}{n^2}}$ where x is a data value, n is the total number of specimens tested, and $\bar{x}$ is the mean of all the data values.

reported average of five units tested in accordance with ASTM C 67 (ASTM, 1999). These manufacturer reported values in Table 2 can be compared with the results of tests conducted for this study shown in Table 7 and discussed below.

2.1.1 Compression Brick Test

The bricks' compressive strength was determined by testing five bricks in accordance with ASTM C 67 (ASTM, 2001). The bricks were saw cut in half, capped and loaded perpendicular to the bed. Unlike the ASTM standard, the bricks were not dried so that the strength value was representative of conditions in the wall panels. Also, the bricks were not shellacked, but were capped with hydrastone. Compressive strength, C, is taken as

$$C = \frac{W}{A} \tag{1}$$

where W is the maximum load and A is the gross area. The test setup is shown in Figure 7 (a).

2.1.2 Split Tension and Modulus of Rupture Brick Test

Five specimens were tested using the split-tension test according to ASTM C 1006 (ASTM, 2001). Each brick is loaded perpendicular to the bed via two long metal

Table 2: Reported brick properties

Gross Area		29.50 in.^{2}
Net Area		25.08 in.^{2}
Compressive Strength	Gross	6933 psi
	Net	8155 psi
Absorption	24 Hr. Cold Soak	6.04
	5 Hr. Boil	9.61
Saturation Coefficient		0.63
Initial Rate of Absorption (IRA)		40.41

Figure 6: Typical brick.

rods that lay across each brick face as shown in Figure 7 (b). The rods' diameter is ¼ in. and it is at least as long as the brick width. The splitting tensile strength, T, is determined using the equation

$$T = \frac{2P}{\pi LH} \tag{2}$$

where P is the maximum applied load, L is the net split length parallel to the rods, and H is the brick height. The test creates a nearly constant tensile stress that results in strength values that are close to but slightly higher than direct tension tests (Drysdale, 1994).

The bricks' modulus of rupture is related to the bricks' tensile strength. This modulus of rupture (flexure) test was conducted in accordance with ASTM C 67, except that the five brick units were not dried so that the strength value was representative of conditions in the wall panels (ASTM, 2001). ASTM calculates modulus of rupture, S, as

$$S = \frac{3W(L/2 - x)}{bd^2} \tag{3}$$

where W is the maximum applied load, L is the span length, b is the net width, d is the brick height, and x is the average distance from the mid-span of the specimen to the plane of failure measured in the direction of the span along the centerline of the bed surface subjected to tension. The test setup is shown in Figure 7 (c).

2.1.3 Discussion of Brick Test Results

All three brick tests had very high COV's (18% to 25%). This high variation is expected because the bricks are very brittle and highly sensitive to minor flaws. Also, poor quality bricks were chosen intentionally to better represent brick qualities present in historic buildings. These bricks were not manufactured to bear large loads and so, the high strength variability is not unreasonable. Still, the average tested compressive

strength was about 40% lower than the manufacturer's reported values (see Table 2), though some reduction in strength is expected since the compression tests for this research were performed without drying the bricks.

The modulus of rupture (flexure) test gives some indication of the tensile strength of the brick. The ability of the test to predict the tensile strength is limited by the relatively small span length (6 5/8 in.) to brick height (2 ¼ in.) ratio. Because of the deep beam action, significant arching action may have occurred. This arching action as well as the fact that a smaller fraction of the section is being highly stressed explains why the average modulus of rupture value (794 psi) is significantly greater than the average tensile strength value (516 psi) determined using the split tension test. The average distance, x, from the mid-span of the specimen to the plane of failure, measured in the direction of the span along the centerline of the bed surface subjected to tension, was as large as 1-1/16 in. This large value demonstrates that small flaws can greatly influence brick strength, since clearly, failure did not always occur at the cross-section with the largest bending moment. Also, the COV was very large (25%), suggesting that the conclusions drawn from panel tests are limited by the high variability in the strength of the bricks. Bricks generally failed in a brittle manner with a single visible crack near the center. However, one brick began losing load carrying capacity in a rather ductile manner with no visible cracks. According to the two tension tests, the brick net tension strength is 10% to 20% of the compressive strength.

2.2 Mortar

In order to observe two potential failure modes, two mortar types were used in the panels such that in the wall panels with weak Type N mortar, failure should initiate in the

brick mortar interface, and in the specimens with strong Type M mortar, failure should initiate in the bricks. In masonry buildings, the mortar or brick/mortar interface is almost always the weakest link as is recommended by the non-mandatory section of ASTM C 270 (Sathish, 2000). Mortar was mixed in accordance with the standards for Type N and M cement-lime mortars as stated by ASTM C 270 (ASTM, 2001) and shown in Table 3. Actual mix properties used in the test specimens are indicated in Table 4. Natural sand was obtained from Teichert, Inc.'s Perkins Plant in Sacramento, California. This sand was sifted through a No. 8 sieve in the lab to obtain the gradation in the right column of Table 5, which meets the ASTM requirements shown in the left column of Table 5.

Table 3: ASTM C270 mortar proportion specification and property requirements

Mortar Type	**Proportion By Volume**			**Average Compressive Strength at 28 days, Minimum**
	Cement	Lime	Sand (damp and loose)	
M	1	¼	Not less than 2 ¼ and not more than 3 times the sum of the separate volumes of cementitious materials	2500 psi
S	1	Over ¼ to ½		1800 psi
N	1	Over ½ to 1 ¼		750 psi
O	1	Over 1 ¼ to 2 ½		350 psi

Table 4: Actual mix proportions

Mortar Type	**Proportion By Volume**		
	Type I/II Portland Cement	Type S, Hydrated Lime	Sand (damp and loose)
M	1	0.25	3.5
N	1	1	6

Table 5: Sand gradation

Sieve Size	**Percent Passing**	
	ASTM Natural Sand Grading Specification	Actual Grading Used for Specimens
4.75 mm (No. 4)	100	100
2.36 mm (No. 8)	95-100	100
1.18 mm (No. 16)	70-100	90
600 μm (No. 30)	40-75	53
300 μm (No. 50)	10-35	18
150 μm (No. 100)	2-15	3
75 μm (No. 200)	0-5	1

The water-cement ratio was approximately 0.6 and 0.9 by weight for the mortar types M and N, respectively, though the exact amount of water was adjusted to maintain proper consistency for workability and adequate bonding of the mortar to the brick. ASTM C 270 recommends using the maximum amount of water appropriate for proper consistency, and in practice, the exact water content is generally adjusted by the mason as was the case for the construction of the walls for this experiment (Sathish, 2000).

2.2.1 Mortar Tests

Various mortar tests were conducted on cylinders of mortar to evaluate the strength of the mortar used to join the bricks. The cylinders were 3 in. in diameter and 6 in. in length. They were compacted with a rod after each third of the cylinder was placed and were further consolidated with a vibration table. The cylinders were tested according to ASTM C 496 after 7 days of curing in a fog room (ASTM, 1996). First a split tension test was performed in which the cylinders were subjected to a compressive load parallel to the longitudinal axis of the cylinder. Second, the compressive strength of the mortar was determined according to ASTM C 39 in which the cylinders were loaded axially (ASTM, 2001).

Mortar compression tests showed that Type M mortar was 3.5 times stronger in compression than Type N mortar after 28 days curing. The 28-day tests were approximately 1.5 times stronger than the tests taken at 7 days. In tension, Type M mortar was only 2.6 times stronger than the Type N mortar. The variation in the mortar test results was significantly lower than the brick tests.

2.3 Masonry Prism Test

Masonry prisms consisting of three brick units stacked on top of each other were tested in compression according to ASTM E 447 (ASTM, 1991). Five masonry specimens were constructed for each mortar type. The prisms were cured 21 days in the fog room followed by 7 to 8 days at room temperature before testing. The prisms were loaded at a rate between 50 and 60 kips per minute.

The prisms with Type M mortar were 1.2 times stronger than the prisms with Type N mortar indicating the composite strength of the prisms is dependent on the type of mortar used. Still, the difference between the two mortar types is not nearly as great as when only mortar was tested, suggesting that both the brick and mortar strengths contribute to the overall strength of the masonry prism. All the prisms failed along two planes lengthwise roughly along the line of the cored openings. Debonding between bricks and/or cracking along the mortar brick interface did not exist. A typical failure is shown in Figure 7 (d). Also, the COV for the prism tests was much lower than the COV for the bricks when tested alone. This reduction in variation suggests that the mortar or the mortar-brick interface governed the prism strength rather than just the brick strength.

2.4 Direct Shear Test

Direct shear tests were performed using the same bricks and the same mortar as part of a separate research project (Tsang, 2003). The direct shear tests were performed using assemblies of four bricks depicted in Figure 8. Two configurations were tested to observe the difference in shear strength between the cored bed-joint surface and the head

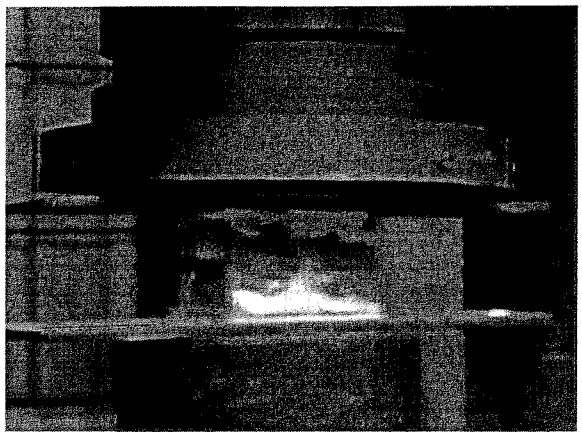

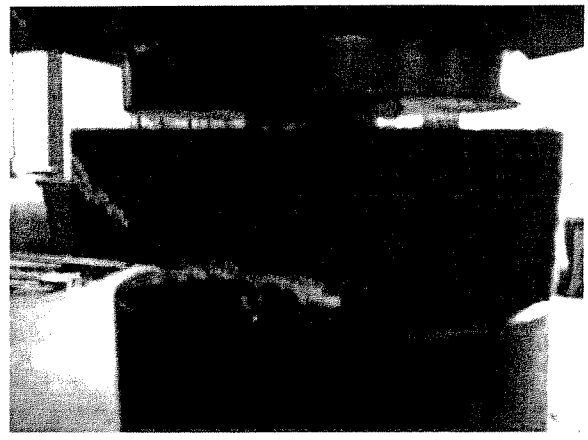

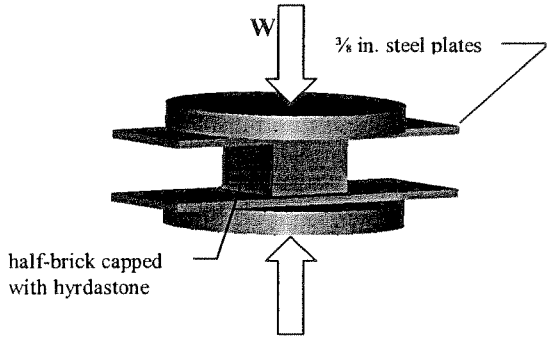

(a) Compression test.

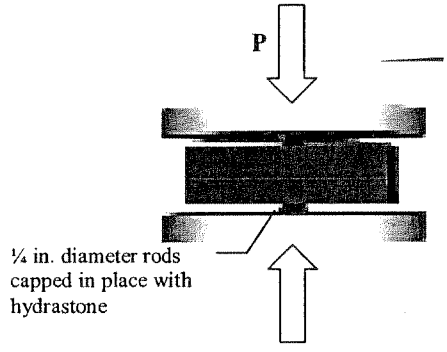

(b) Split tension test.

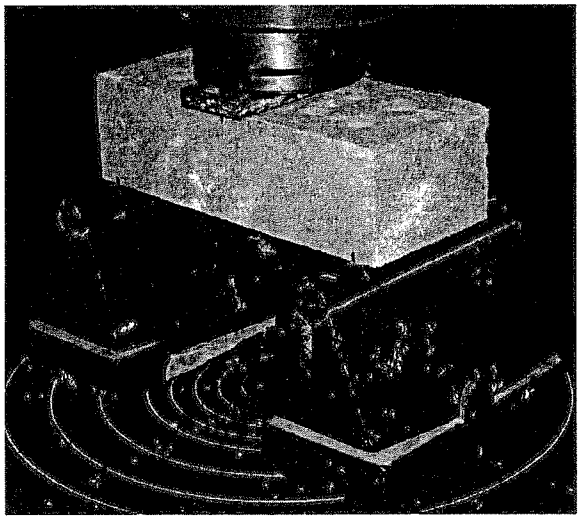

(c) Modulus of rupture (flexure) test.

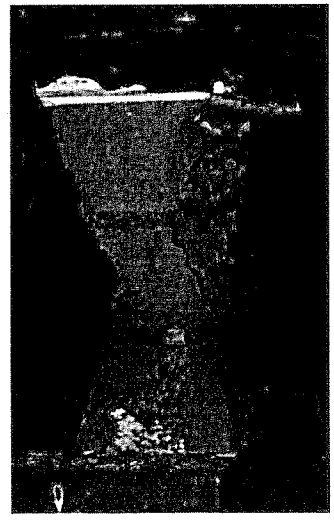

(d) Masonry prism test.

Figure 7: Brick and prism tests.

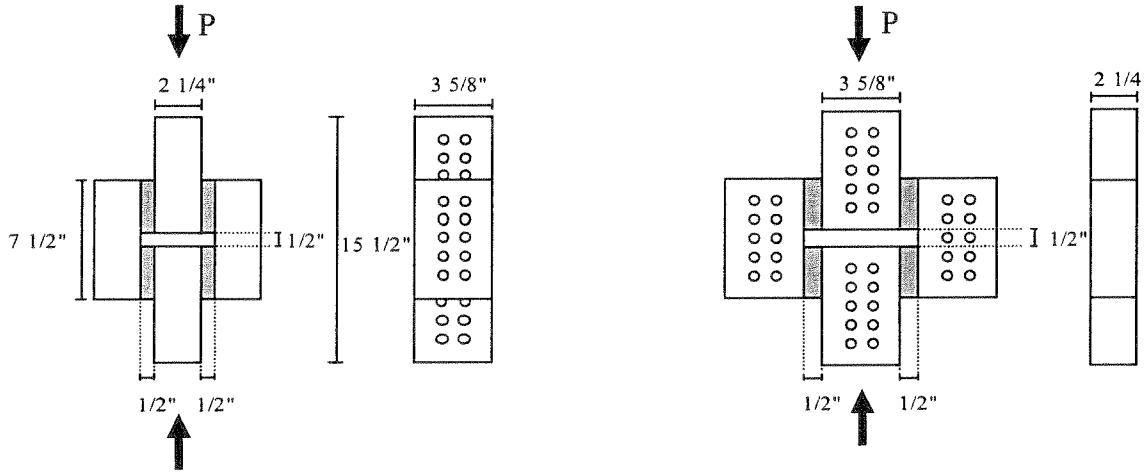

(a) Cored face specimens (a) Smooth face specimens

Figure 8: Configuration of direct shear test (Tsang, 2002).

joint. In the configuration depicted in Figure 8 (a), the bricks are joined along the bed surface. In the test depicted in Figure 8 (b), the bricks are joined along their sides, which mimic the shear strength at the head joints. A load, P, was applied to the center bricks and the gross shear stress was calculated as

$$\tau = \frac{P/2}{A_g} \tag{4}$$

where A_g is 12.7 in.^{2} and 7.9 in.^{2} for the cored face and smooth face, respectively. The shear stresses are shown Table 7. From the results it is evident that the cores contribute significantly to shear strength, because the mortar sinks into the cores and interlocking resists shear forces. The results also show that Type M mortar has greater bond strength than Type N mortar, but that the bond strength of the Type M mortar is much more variable. This increase in bond strength corresponds with Boyton's study in which cross-couplets were used to show that bond strength increases with increased Portland cement content and decreases with lime cement content (Tsang, 2002 and Boyton, 1964). In addition the Type M mortar is more susceptible to flaws due to its brittle property, so the higher variation is understandable.

2.5 Fiber Reinforced Polymer

Professional contractors with experience in retrofitting projects applied two glass fiber reinforced polymer (FRP) sheets to one side of the brick panels. Hex-3R Wrap 101G manufactured by Hexcel Corporation was used in combination with Sikadur Hex 300 high modulus, high strength, impregnating resin to form a glass fiber reinforced polymer laminate. The manufacturer, Sika, reported material properties shown in Table 6. The tensile and shear properties of the Sikadur Hex 300 and Hex-3R Wrap 100 Laminate were determined using ASTM D 3039 and D 3518, respectively (ASTM, 2000 and ASTM, 2001). Calculations of FRP design strength for structural engineering applications can be made using either the fiber properties or the laminate properties. Throughout this report, calculations are made according to the laminate properties. The ply thickness of 0.04 in. refers to the overall laminate.

Table 6: Reported FRP properties[a,b]

E-glass Fiber Properties	
Tensile Strength	330,000 psi
Tensile Modulus	10,500,000 psi
Density	2.54 g/cc
Elongation	4.0%
Sikadur Hex 300 and Hex-3R Wrap 101 Laminate Properties	
Tensile Strength	44,100 psi
Tensile Modulus	2,270,000 psi
Shear Strength	9,000 psi
Shear Modulus	470,000 psi
Poisson Ratio	0.189
Elongation	2.37%
Ply Thickness	0.040 in.
a. Properties after standard cure followed by standard post cure (70-75°F– 5 days, 48 hours at 140°F). b. Properties are given for a single ply though two plies were used on the panels.	

Table 7: Material test results

	Curing Period	Specimens Tested	Average Strength	COV
Brick Compression Test		5	4341 psi	24%
Modulus of Rupture (Flexure) Brick Test		5	794 psi	25%
Brick Split Tension Test		4	516 psi	18%
Mortar Compression Test				
Type N				
	7 days	3	736 psi	2%
	28 days	3	1179 psi	2%
Type M				
	7 days	3	2910 psi	0%
	28 days	3	4155 psi	2%
Mortar Split Tension Test				
Type N				
	7 days	3	113 psi	9%
	28 days	3	186 psi	3%
Type M				
	7 days	3	393 psi	13%
	28 days	3	487 psi	9%
Masonry Prism Test				
Type N	28 days	5	2906 psi	4%
Type M	28 days	5	3472 psi	4%
Direct Shear Test				
Type N: Cored Face		2	156 psi	11%
Type M: Cored Face		2	232 psi	33%
Type N: Smooth Face		2	106 psi	5%
Type M: Smooth Face		2	182 psi	42%

3 CONSTRUCTION AND TEST SETUP

3.1 Masonry Panel Construction

Brick panels, 30 in. by 30 in. square, were constructed in a laboratory environment. Single-wythe panels were constructed in the pattern shown in Figure 4 (d) with half blocks at every other row end. Vertical joints were approximately 10/32 in. or 8/32 in. and horizontal bed joints were approximately 9/32 in. As is common in URM buildings (see the brick pattern in Figure 5), three-wythe panels were constructed with headers placed every sixth course in the common bond brick pattern as shown in Figure 9.

3.2 FRP Application

In preparation for application of the FRP, the brick wall was sand blasted thoroughly to remove excess mortar and create a flat surface. The panel was then air blown to remove sanded clay particles. Next, a filler mixture of Cabosil (a compound of

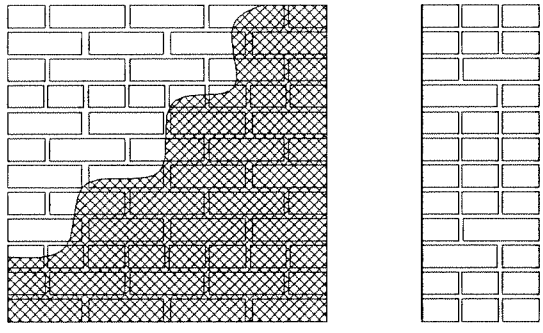

Figure 9: Three-wythe brick panel with a common bond header line every sixth course. Part of the FRP sheet is visible (FRP strands not to scale).

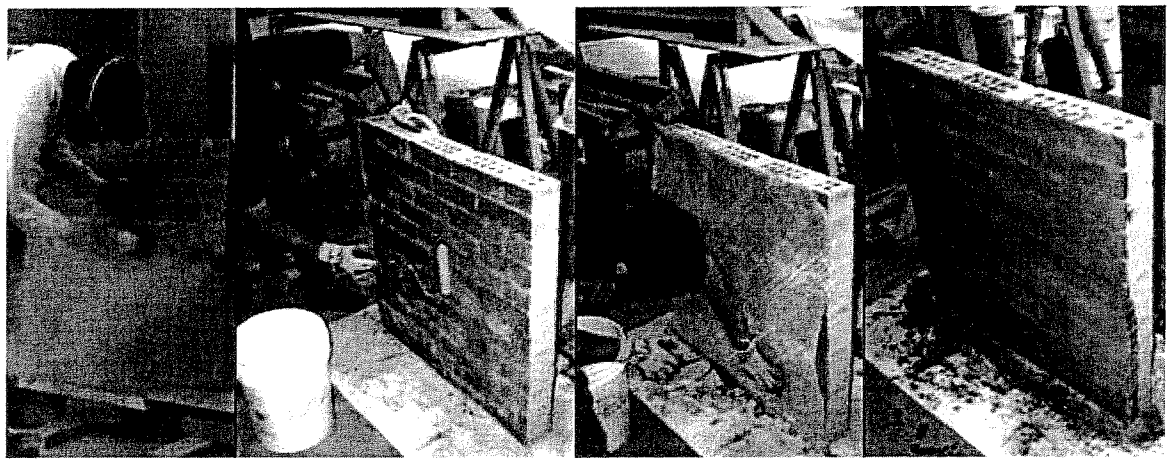

Figure 10: Process of applying FRP.

fine aggregates) and Sika epoxy resin was used to fill in large pores in the bricks and mortar. The Sika epoxy resin was spread onto the entire panel using rollers. The first FRP sheet was placed on the panel with the fibers aligned at ±45 degree angles to the edge as shown in Figure 9. The contractors then rolled more resin over the first sheet to remove air gaps. The second ±45 degree sheet was placed on the first resin-covered sheet and again covered with more resin and smoothed and pressed to remove any air gaps. Figure 10 shows the major steps of the retrofitting process.

3.3 Setup of Diagonal Tension (Shear) Test

The effectiveness of the retrofitting scheme was evaluated using ASTM E 519, The Standard Test Method for Diagonal Tension (Shear) in Masonry Assemblages (ASTM, 1988). To create the loading condition shown in Figure 4 (d), the panel corners were capped with hydrastone and placed into steel loading shoes. The placement was checked carefully to ensure the wall was vertically plumb and loading shoes were placed evenly. Figure 27 in the Appendix contains details regarding the loading shoe dimensions. The panel was subjected to monotonic quasi-static loading at an average rate of 6.6 kips

per minute for the one-wythe specimens and 21.7 kips per minute for the three-wythe specimens.[2]

3.4 Instrumentation

After placing the panels in the test machine, small holes were drilled into the brick on each side of the panel near the corners where tension and shear stresses would be small. Threaded rods were inserted into the holes and embedded with hydrastone. Displacement transducers were placed on the rods to measure horizontal and vertical displacements on each side of the specimen. The gage length of each device was 26 in. The instrumentation setup is shown in Figure 11. Inserting the rods into the brick had minimal effect on behavior since cracks never initiated at the rod. The out-of-plane distance from the wall to the gage was measured, so that by comparing displacements on each side of the wall, wall curvatures could be estimated. For some specimens, out-of-plane displacements were measured at the center of the wall, but because the measured values were very small, they are not discussed in this report. Another displacement transducer measured the displacement of the loading head and a load cell measured the force applied to the specimen.

[2] The loading rate was calculated by dividing the load at yield by the time to yield. The three-wythe wall was loaded at a rate approximately three times the rate of the single wythe wall to maintain a constant stress rate.

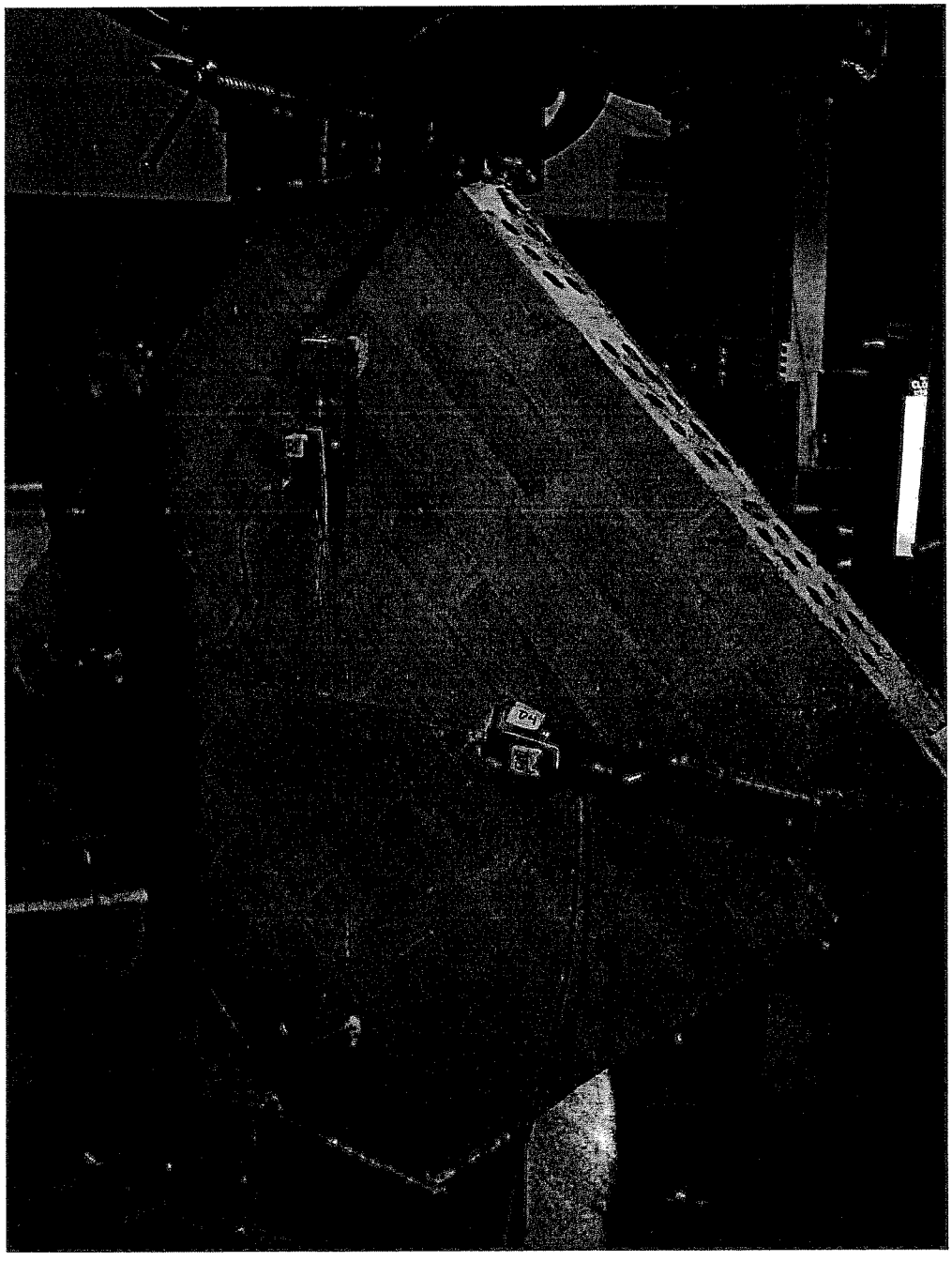

Figure 11: Diagonal tension test with instrumentation.

4 RESULTS

The results of the diagonal tension tests are shown in two forms. Figure 12 depicts shear force versus drift, where shear force is normalized by the wall's original thickness and Figure 13 depicts brick shear stress versus shear strain. The three subplots in each figure show the effect of retrofitting on the three different variable combinations considered. The shear force normalized by thickness is defined as

$$\frac{V}{t} = \frac{P}{t\sqrt{2}} \tag{5}$$

where t is the thickness of the wall and P is the applied load. Figure 4 (c) shows a free body diagram of the shear force. It is clear from the diagram that the bricks near the center of the panel experience a compression and shear load. In a URM wall, axial load would develop due to gravity, overturning moment, and/or vertical ground accelerations, whereas the shear load would be transferred to the wall from the inertia effects of floor or roof diaphragms (Figure 4 (a)). The wall's drift, δ, is calculated according to the formula

$$\delta = \frac{L - \sqrt{\left(\sqrt{2}L - \Delta_u\right)^2 - L^2}}{L} \tag{6}$$

where L is the average gage length of the two vertical displacement transducers and Δ_u is the average of the magnitude change in length of each vertical gage. Horizontal gage length changes are not considered since the measurement becomes unrepresentative at high displacements due to cracking and large curvatures as discussed later with reference to Figure 22. The drift equation is only a rough approximation of the actual panel

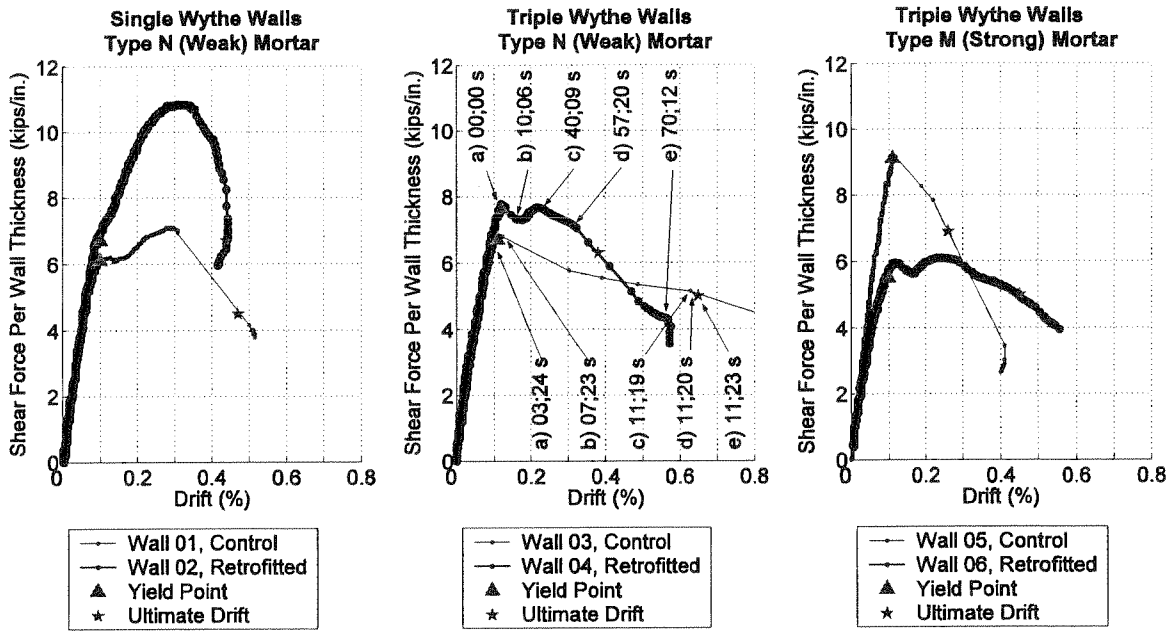

(a) (b) (c)

Figure 12: Shear Force versus Drift relationships.[3]

deformation. The equation assumes that the length of each panel edge remains constant and that the wall shortens vertically the same distance that the wall expands horizontally. The latter assumption is not entirely accurate since displacement transducers indicate that the vertical and horizontal displacements are not of the exact same magnitude, but on average the above equation gives a reasonable estimate of the performance of a brick panel.

Figure 13 compares the brick shear stresses (defined later) with shear strains. Shear strain, γ, is determined from changes in the gage lengths and is calculated using the ASTM equation

$$\gamma = \frac{\Delta V + \Delta H}{g_{avg}} \tag{7}$$

[3] The labeled points in Figure 12(b) represent time after yielding and correspond with photos in Figure 16 and Figure 17 as discussed later. Time units are ([seconds]; [1 second / 30]), because each video frame lasts 1/30 seconds.

where ΔV and ΔH are the average changes in gage length taken on both sides of the specimen in the vertical and horizontal direction, respectively. g_{avg} is the average gage length, though all lengths are the same within ±0.25 in. In calculating the shear strain, uniform strain across the thickness of the wall and the FRP is assumed. Debonding of the FRP was never observed in areas where displacements were measured, so it is reasonable to assume the strain in the FRP was the same as that in the bricks at least until the point of cracking. On retrofitted walls, measured strains did vary significantly on both sides of the walls, because the walls curved concave-in around the FRP (see Figure 21), but by taking the average of both sides, a reasonably characteristic shear strain is determined.

Shear stress, τ, in unretrofitted specimens is simply calculated by

$$\tau = \frac{\mathrm{P}}{\sqrt{2}} \frac{1}{A_n} \tag{8}$$

where A_n is the net cross-sectional area of the wall defined as follows

$$A_n = nwt \tag{9}$$

where w is the wall width (30 in.), t is the wall thickness (3.625 in. and 11.625 in. for the single-wythe and triple-wythe walls, respectively), and n is the percentage of the wall cross-section that is solid (84% and 85% for the single-wythe and triple-wythe walls, respectively).

Reporting the brick shear stresses in the retrofitted specimens is more complex than in the unretrofitted specimens, because some force is resisted by the FRP. The shear stiffness of the FRP-epoxy laminate is reported in Table 6. This shear stiffness is obtained from tests performed in accordance with ASTM D3518 (ASTM, 2001). These tests measure shear stiffness from a stress-strain state that is nearly identical to the stress-strain state present in the retrofitted panel as shown in Figure 4 (e) (Petit, 1969). The shear

stress-strain relationship of the FRP-epoxy laminate is nonlinear. The stiffness is measured between 2000 and 6000 microstrain. Strains in the reported tests reached values both below and above this range. For strains in the panels' elastic region, it may be more accurate to use a slightly higher stiffness value and for strains greater than this range, a slightly lower value is more appropriate. However, the actual contribution of the FRP to the stiffness of the panel is greatly affected by many complex factors: the bond with the brick; the interaction of the FRP with the resin; and the exact strain distributions in the wall. Because calculations of the brick shear stress are already approximations of the actual complex stress state, using a single value for shear modulus will not significantly affect the already approximate calculation. By using this method, the stresses in the bricks can at least be compared consistently for each specimen. The assumption that the laminate's shear stress-strain relationship is linear is reasonable since the stress-strain curve does not plateau until strains much higher than those experienced in the wall tests. The stress in the FRP, τ_{FRP}, can be estimated by

$$\tau_{FRP} = G_{FRP}\gamma_{avg} \tag{10}$$

where G_{FRP} is the shear modulus of the FRP (470,000 psi) and γ_{avg} is the average shear strain across the section. The FRP shear stress is based on the FRP's shear strain, which is measured from displacement transducers that measure the average strain across the transducer gage length. After the bricks or mortar crack, the shear strain is no longer constant across the width of the walls. The walls curve out of plane and the actual shear strain in the FRP may be significantly different than the strain calculated using measurements from the transducer on the side with the FRP (see Figure 21). At high strains near failure, the horizontal transducer on the FRP side indicates contraction of the

wall while the horizontal transducer on the bare side indicates the expected expansion. The reported contraction occurs because the brick wall curves inward, shortening the gage length. Since the transducer is really indicating curvature in the wall and not compressive stresses in the FRP, the FRP stress calculation will be most accurate if the average displacements of gages on each side are used to determine the shear strain. Once the shear stress in the FRP is known, the net shear stress in the bricks, τ_{br}, can be calculated by equilibrium of shear forces as follows

$$V_{br} = V_{total} - V_{FRP} \tag{11}$$

$$\tau_{br} = \frac{P/\sqrt{2} - \tau_{FRP} t_{FRP} w}{A_n} \tag{12}$$

where $V_{FRP} = A_{FRP}\tau_{FRP}$, $V_{total} = P/\sqrt{2}$, and V_{br} is the calculated shear force resisted by the bricks. Constant shear stress, τ_{br}, is assumed across the wall section. Figure 13 allows direct comparisons of the brick stress and ultimate strains in retrofitted versus unretrofitted walls. Each point on the graph represents measurements that were taken every second. Yield stress and ultimate shear strain are indicated on Figure 13 with large triangles and stars, respectively. The "yield" stress is calculated by determining where the tangent shear modulus first drops below 100,000 psi. This shear modulus value was chosen simply because it resulted in a reasonable yield stress for every specimen. Note that yield here is used to refer to change of stiffness rather than on-set of real plastic deformation. The term "yield" was chosen rather than cracking stress, because sometimes small cracks developed before dramatic changes in stiffness. Also, using the term "yield" is consistent with a later discussion of ductility, which is then defined in the traditional engineering sense using the corresponding "yield" strain. The ultimate strain was

determined by finding the shear strain when the wall's capacity deteriorates to 75% of the yield stress.

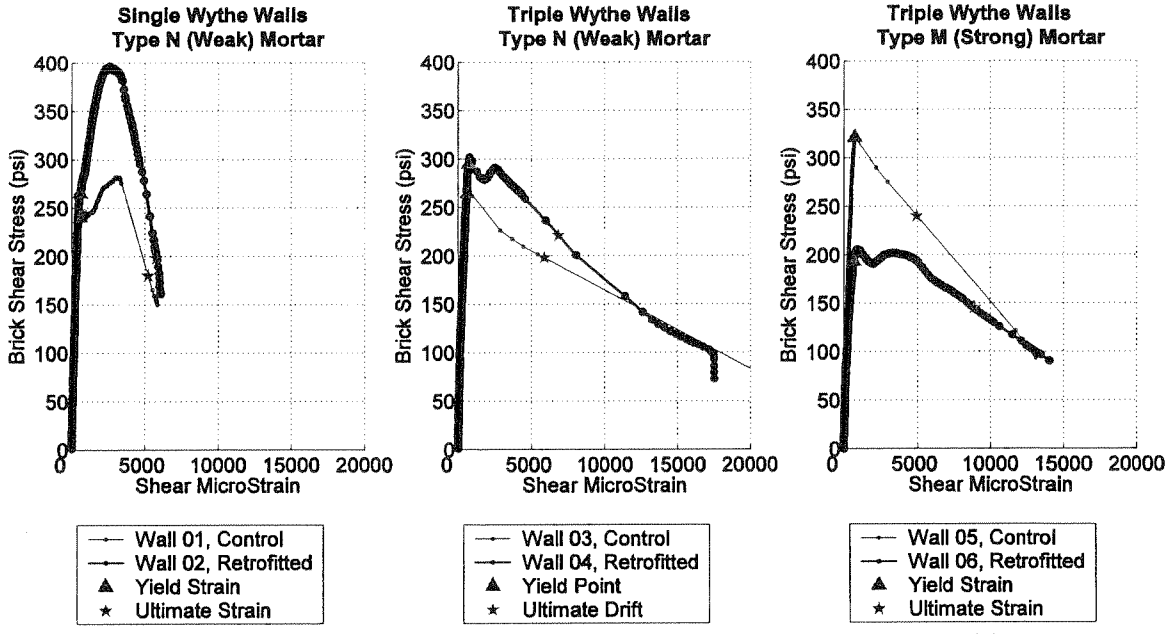

(a) (b) (c)

Figure 13: Shear Strain versus Brick Shear Stress relationships.

5 DISCUSSION OF RESULTS

Figure 12 and Figure 13 show a wide variety of behavior for the six specimens tested, so clearly more tests are needed to confirm definitively the effectiveness of FRP as a retrofit option on one side of a three-wythe URM wall. Still, the results allow a few conclusions to be made. First, Figure 13 shows that the elastic behavior of the panels is not significantly affected by the addition of FRP. Also, the FRP does not seem to greatly enhance the strength of the three-wythe panels. As shown in Figure 14, the triple-wythe retrofitted wall with weak mortar is slightly stronger than the unretrofitted wall, but for the strong mortar, the retrofitted panel was actually much weaker. This inconsistency prevents any general conclusions from being made regarding the FRP's effect on strength of a three-wythe wall. Figure 14 also shows that no conclusions can be made regarding the effect of FRP on ultimate drifts. The retrofitted Wall 4 actually had a lower ultimate drift (as defined above) than the unretrofitted Wall 3.

Wall 1 (single wythe, control) and Wall 2 (single wythe, retrofitted) both yield at about the same drift near 6 kips/in. when initial cracking in the brick is observed. While the unretrofitted wall gains minimal strength after cracking, the retrofitted wall continues to resist load as the FRP bears additional forces, resulting in a maximum load almost twice as large as the yield load. The retrofitted single-wythe wall yielded at about the same point as the control wall, but then continued to gain strength as the FRP continued to carry additional strength. This effect was not observed in three-wythe walls, probably

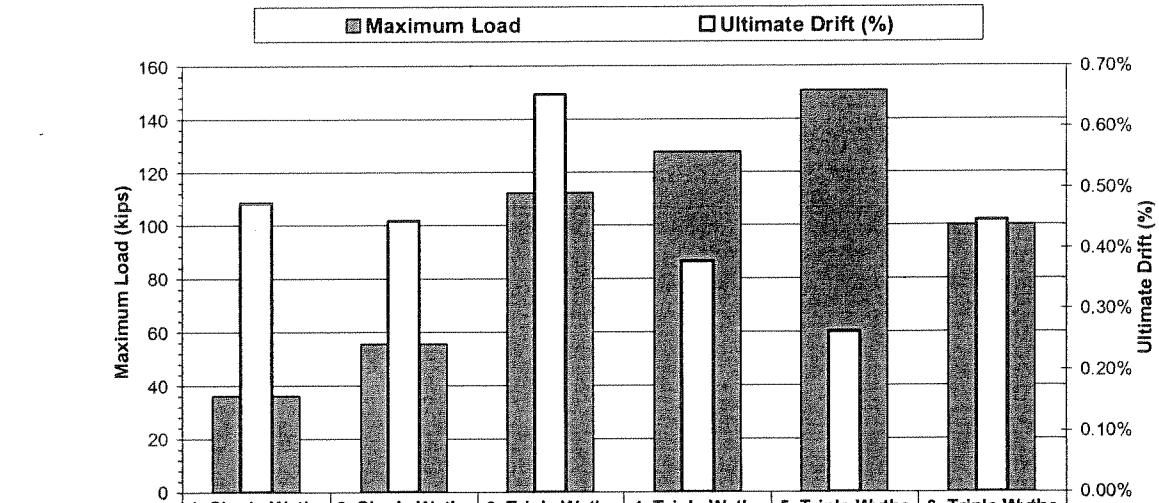

	1. Single Wythe Control, Type N Mortar (weak)	2. Single Wythe Retrofit, Type N Mortar (weak)	3. Triple Wythe Control, Type N Mortar (weak)	4. Triple Wythe Retrofit, Type N Mortar (weak)	5. Triple Wythe Control, Type M Mortar (strong)	6. Triple Wythe Retrofit, Type M Mortar (strong)
Maximum Load	36	56	112	128	151	100
Ultimate Drift (%)	0.47%	0.44%	0.65%	0.38%	0.26%	0.45%

Figure 14: Comparison of ultimate drift and maximum load.

because the FRP could not continue to resist forces after bricks on the opposite side failed.

5.1 Ductility

A comparison of the walls based on ductility yields no definite trends. Using the definitions of yield and ultimate shear strains defined above, the wall ductility with respect to shear strain can be calculated from

$$\mu_y = \frac{\gamma_u}{\gamma_y} \tag{13}$$

where γ_u and γ_y are the ultimate and yield shear strains, respectively. The ductility of the walls ranges from 6.6 to 12.7 as shown in Figure 15. The single-wythe retrofitted Wall 2 provides only a small increase in ductility relative to the unretrofitted Wall 1, whereas no change in ductility was observed for the three-wythe walls with weak mortar. The

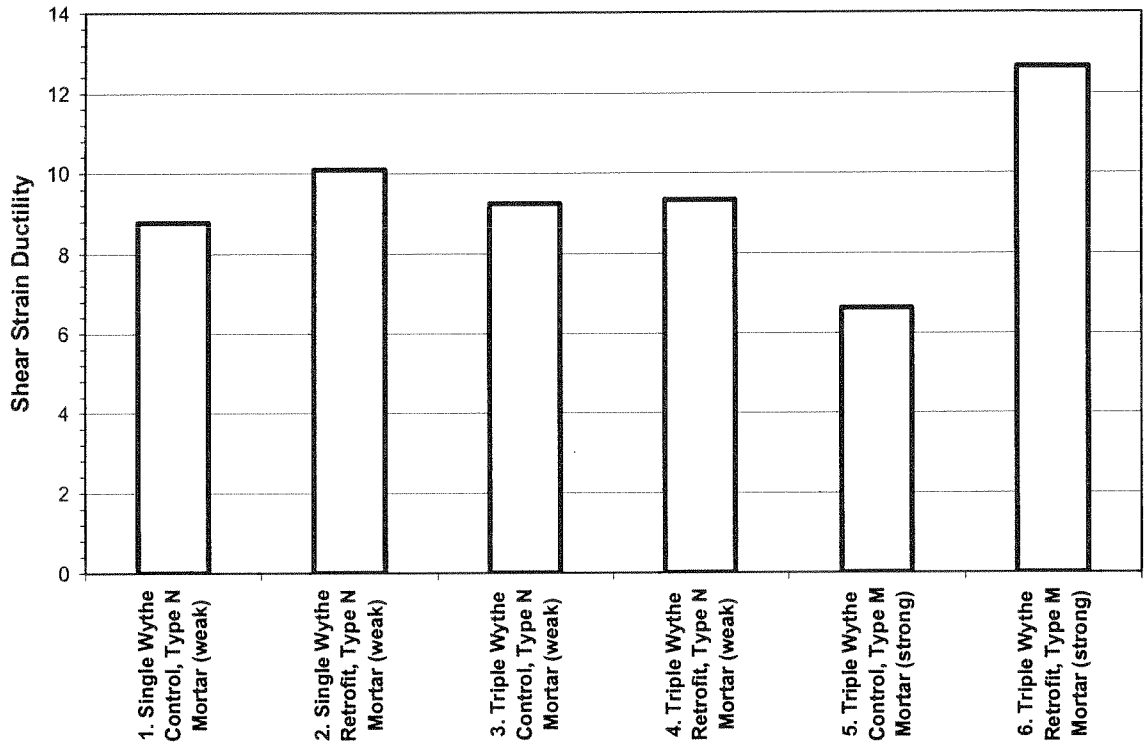

Figure 15: Comparison of shear strain ductility.

retrofitted Wall 6 shows about twice the ductility of the unretrofitted Wall 5, but this comparison is overshadowed by the dramatic drop in strength of the retrofitted wall.

5.2 Strain Rate

The two retrofitted three-wythe walls showed an initial decrease in strength when the first bricks crack followed by a slight increase in capacity as forces shifted to the FRP after the cracked bricks lost stiffness. Rather than resisting additional forces as was the case for the single-wythe walls, the capacity of the retrofitted three-wythe walls continued to deteriorate. The capacity decreased very slowly as indicated by the closely spaced data points in Figure 12. On the other hand, the unretrofitted three-wythe walls cracked and then lost strength quickly as indicated by the widely spaced data points. Standard equations for calculating ductility (e.g. Equation (13)) do not show any

improvement provided by the FRP. It is difficult to justify any improvement provided by the retrofit by simply looking at the plots and ductility calculations. However, observation of the experiments suggests an apparent advantage provided by the FRP. In all cases, the unretrofitted specimens reached an ultimate strength, cracked, and failed catastrophically, whereas the retrofitted specimens developed several cracks and failed gradually.

To quantify this improvement in behavior, Figure 12 (b) is stamped with times

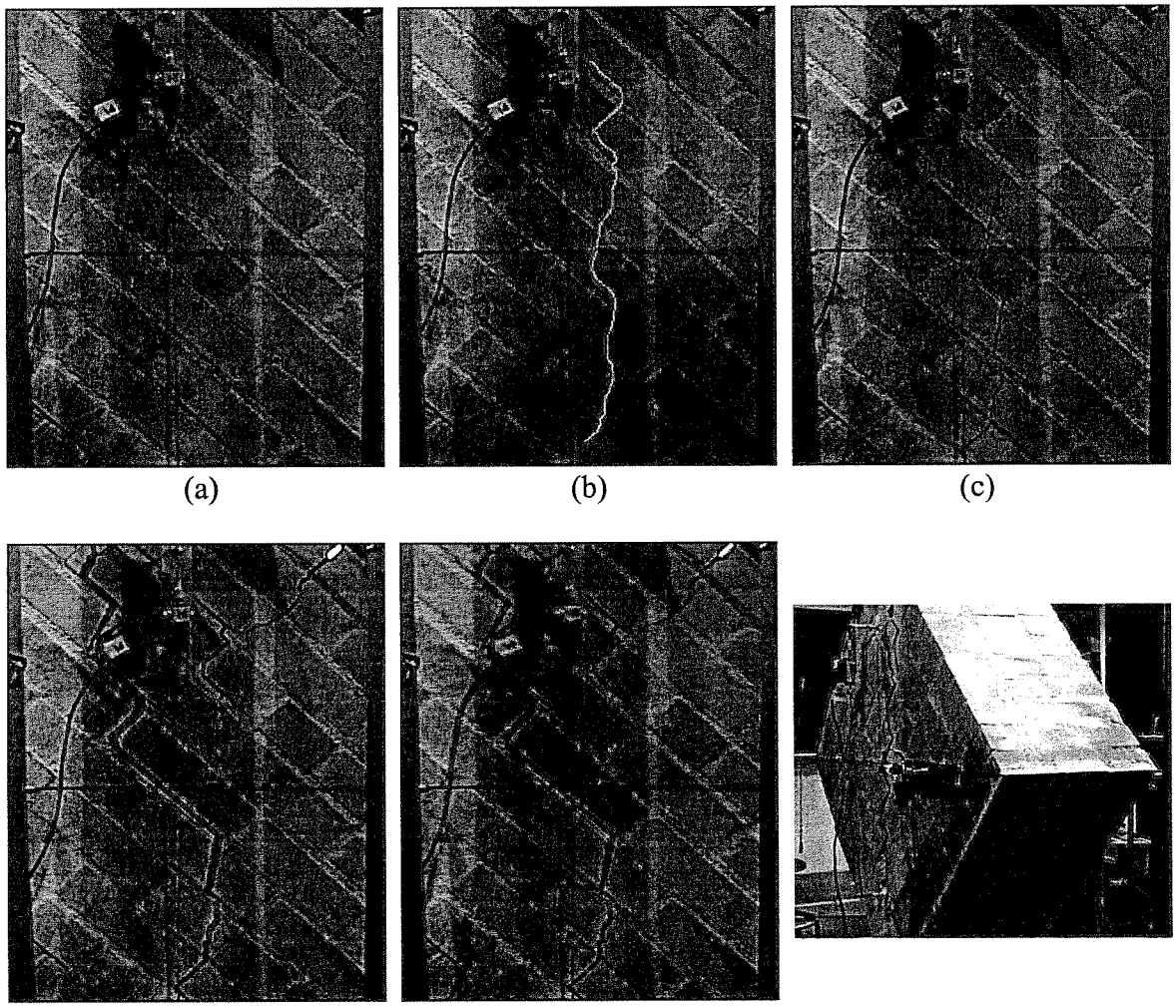

Figure 16: Control Wall 3 (a) 3;24 sec., no visible cracks immediately after yield drift. (b) 7;23 sec., first visible crack (traced in white to the right of actual crack). (c) 11;19 sec., crack widens slightly. (d) 11;20 sec., large crack opens quickly. (e) 11;23 sec., specimen fails. (f) 11;23 sec., crack goes through to the opposite side.

that images were extracted from the video of the control and retrofitted specimen tests. These images are shown in Figure 16 and Figure 17 for the control and retrofitted wall, respectively. Time is set to zero at the point of yielding and time units are ([seconds]; [1 second / 30]), because each video frame lasts 1/30 second. In Figure 16 (b), a small crack forms shortly after yielding of the control Wall 3 (a white line traces the path slightly to the right of the crack). Within four seconds, the crack breaks open violently, and the two sides of the wall completely separate (Figure 16 (d)). A view of the opposite side of the wall is shown in Figure 16 (f).

In Figure 17 (b), a tiny crack propagates shortly after yielding of the retrofitted

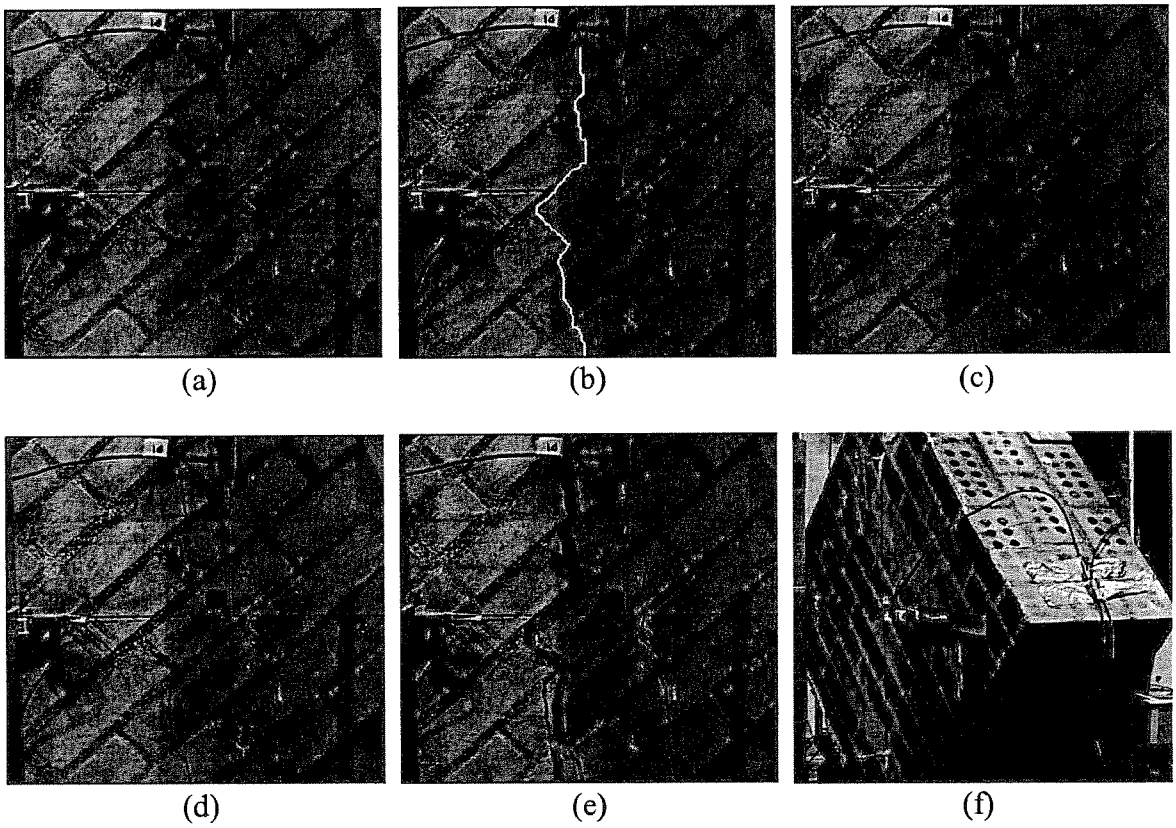

(a) (b) (c)

(d) (e) (f)

Figure 17: Retrofitted Wall 4 (a) 00;00 sec., no visible cracks at yield drift. (b) 10;06 sec., cracks become visible (traced in white to the right of actual crack). (c) 40;09 sec. crack very slowly widens. (d) 57;20 sec., a second parallel crack forms. (e) 70;12 sec., crack widens slowly until test is stopped. (f) 70;12 sec., crack is not visible on the opposite side, which is retrofitted with FRP.

Wall 4. With the FRP retrofit, the crack opens slowly; a second parallel crack opens (Figure 17 (d)); and the wall continues to resist load for 70 seconds, even after the crack becomes very large (Figure 17 (e)). Figure 17 (f) shows the side with the FRP. In Wall 4, the FRP never delaminated from the brick and though the crack propagated through all three wythes, no crack or damage was observed on the FRP face. All three retrofitted specimens exhibited similar behavior.

To quantify this difference in behavior, Figure 18 compares strain rate with brick stress. Strain rate is calculated by

$$\dot{\varepsilon} = \frac{\Delta\gamma}{\Delta T} \tag{14}$$

where $\Delta\gamma$ and ΔT are the shear strain and the time increments, respectively.

The exact relationship between brick shear stress and strain rate is not clear in the graph, nor is it important. The graph simply shows that for all three wall types, the control wall reaches much higher strain rates at particular stresses, as is shown less

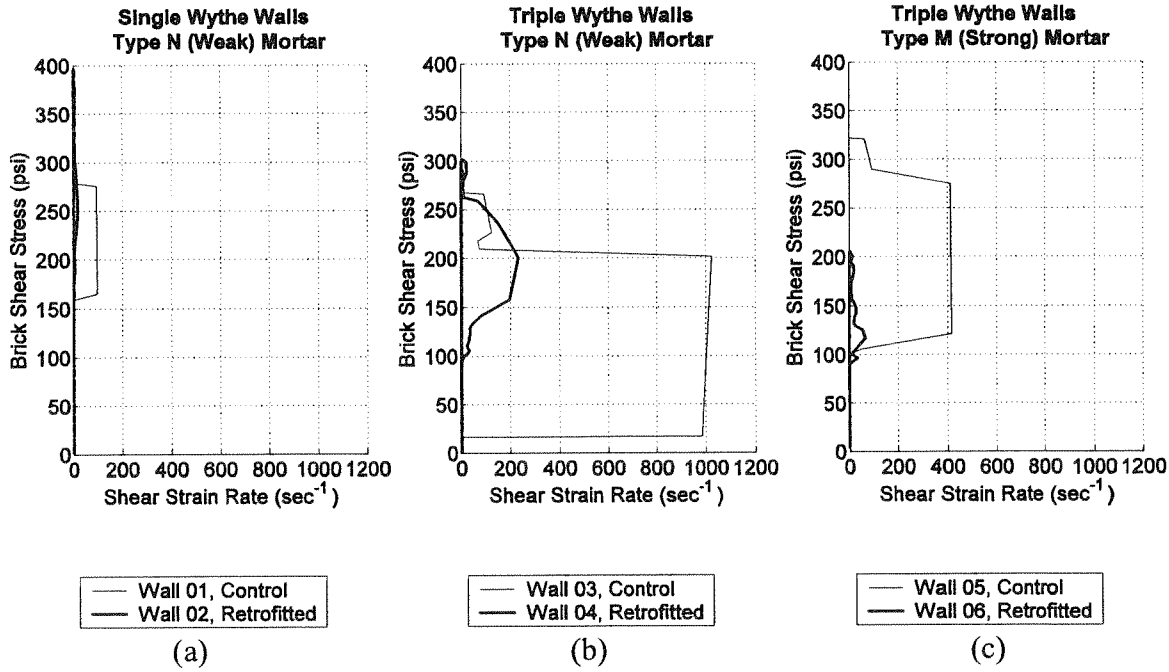

Figure 18: Comparison of shear strain rates.

dramatically by the spacing of data points in Figure 13. The exact strain rate imposed is of course dependent on the loading protocol, but the dramatic difference in the graphs clearly shows that the FRP does improve the walls' ability to withstand forces for longer periods of time. In this context, the FRP clearly affects even a three-wythe wall retrofitted on one side. Therefore, one can expect that FRP reduces the brittleness of multiple-wythe masonry walls under dynamic loading.

5.3 Relative Effect of Mortar Strength

One of the preliminary objectives of this research was to better understand how the retrofitting would be affected by different ratios of brick to mortar strength. Bricks and mortar were chosen with the intention that Walls 1 through 4 with Type N mortar would have much stronger bricks than mortar and failure would initiate in the mortar and zigzag around the bricks. Walls 5 and 6 were intended to have stronger mortar than brick and fail in the brick first and crack directly through the bricks. Unfortunately the bricks proved weaker than expected, and the actual results were not as clearly distinguishable as originally intended. It proved difficult to determine exactly where cracks in the wall initiated. Reviewing the videos of the experiments revealed that in one frame, no cracks were visible and in the next frame ($1/30^{th}$ of a second later), a crack was present across the entire central portion of the wall. Consequently, it was difficult to determine where cracks initiated. Once the crack did form, the crack propagation was significantly different for the two types of mortar. After removing the loading shoes and separating the two fractured pieces, the difference in crack propagation became apparent. Figure 19 and Figure 20 show the two three-wythe control walls with weak Type N and strong Type M mortar, respectively. Though some exceptions exist, it is clear from the two photographs

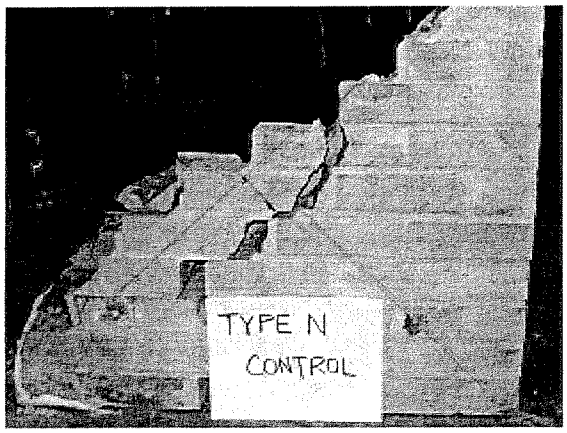

Figure 19: Zigzag crack pattern of the unretrofitted Wall 3 with weak mortar (Type N).

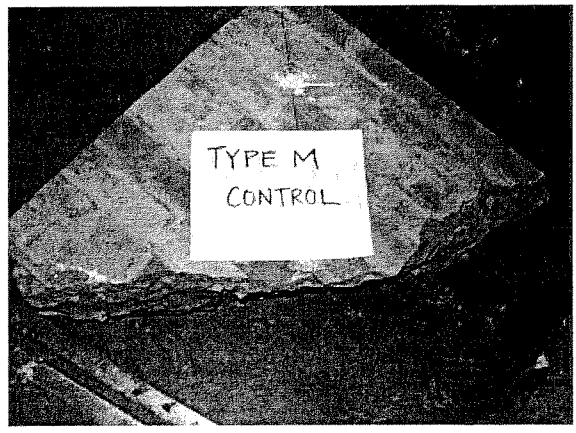

Figure 20: Continuous crack pattern of the unretrofitted Wall 5 with strong mortar (Type M).

that the crack in the wall with weak mortar traveled around the stronger bricks, and in the wall with the strong mortar, the crack propagated directly through the bricks.

It is difficult to determine exactly how the effect of the FRP varied for varying mortar to brick ratios. It is clear from the material tests that the Type M mortar is stronger, but the Type M mortar is also more brittle and consequently more sensitive to flaws. In addition, the higher cement to lime ratio of the Type M mortar reduces its workability, which may also increase the occurrence of flaws in the brick-mortar interface. This brittleness and poor workability may explain why Wall 6 had the lowest load carrying capacity of all four three-wythe specimens. Without the FRP, this flaw could be catastrophic in an actual earthquake loading. However, the FRP allowed the wall to reach large strains despite the early onset of cracking. This increased ductility (evident from Figure 15) may be a very beneficial attribute of the FRP retrofitting technique. It shows that even if a historic wall has a large undetected flaw, the FRP can increase this wall's ductility, which may allow the wall to maintain its gravity load carrying capacity in a major earthquake.

5.4 Test Limitations

Several important test limitations prevent broad conclusions from being made regarding the effectiveness of the FRP in limiting damage in actual buildings subjected to seismic ground accelerations.

5.4.1 Variability

Limitation of resources allowed only six specimens to be tested. Even if six exactly similar specimens were tested, considerable variation in results could occur because the materials and the construction practices were imperfect as in real construction situations. The bricks themselves vary in strength as discussed above. In addition, construction of the walls is an imperfect art, and even the most experienced bricklayer is unlikely to lay each brick exactly the same. Students who constructed the walls were well trained and very high standards of accuracy and precision were pursued, but some degree of variation in workmanship was unavoidable.

5.4.2 Curvature and Eccentricity

Another important limitation of the test was the actual size of the tested panels. Over the height of a larger wall, the FRP may be expected to have an even more significant impact on the behavior of the three-wythe URM. Furthermore, the stresses across the three wythes of bricks and two layers of FRP may not have reached a stress distribution typical in a prototype wall, because the loading shoes were located relatively close to the location of peak tensile stresses. Substantial flexing of the wall about the vertical axis may also significantly affect the drift capacity of the wall. Curvatures in the wall were measured using the difference in displacements of the two horizontal

transducers (one on each side of the wall). The curvature about the vertical axis is calculated from

$$\kappa_{Vert.\ Axis} = \frac{\Delta_{H1} - \Delta_{H2}}{Total\ Thickness} \tag{15}$$

where Δ_{H1} and Δ_{H2} are the change in gage length *g_h1* and *g_h2* of Side 1 and Side 2, respectively as shown in Figure 21. Figure 22 shows the curvature about the vertical axis is much greater in the specimens retrofitted with FRP. The curvatures about the horizontal axis are represented by dashed lines in Figure 22 and are calculated in a similar way to Equation (15) using vertical displacements instead of horizontal. The curvatures about the horizontal axis also appear greater for specimens retrofitted with FRP, but this curvature is much smaller that that about the vertical axis since no horizontal cracks develop. The non-zero curvatures about the horizontal axis in control Wall 3 and to a lesser extent Wall 5 represent either small eccentricities in the placement and/or construction of the wall or differences in brick/mortar strength or stiffness across the walls' thickness. The dashed line for Wall 1 coincides with the x-axis.

In the photograph of Section B-B in Figure 21, a yardstick lies horizontally on the two pegs used to hold the instrumentation measuring gage length, *g_h1*. The curvature of the non-FRP surface of the retrofitted Wall 6 is evident from the gap that develops between the straight yardstick and the curved panel surface. On a prototype wall, such large curvatures may increase the likelihood of splitting off of the exterior wythe as shown in Figure 23. Also, in the experiments, loads were applied evenly across the thick wall using stiff steel loading shoes (details in Figure 27 of the Appendix). In a prototype building, walls may be loaded eccentrically by beams framing in from the interior floor diaphragms. This eccentricity may cause further curvature. Also, a concentrated

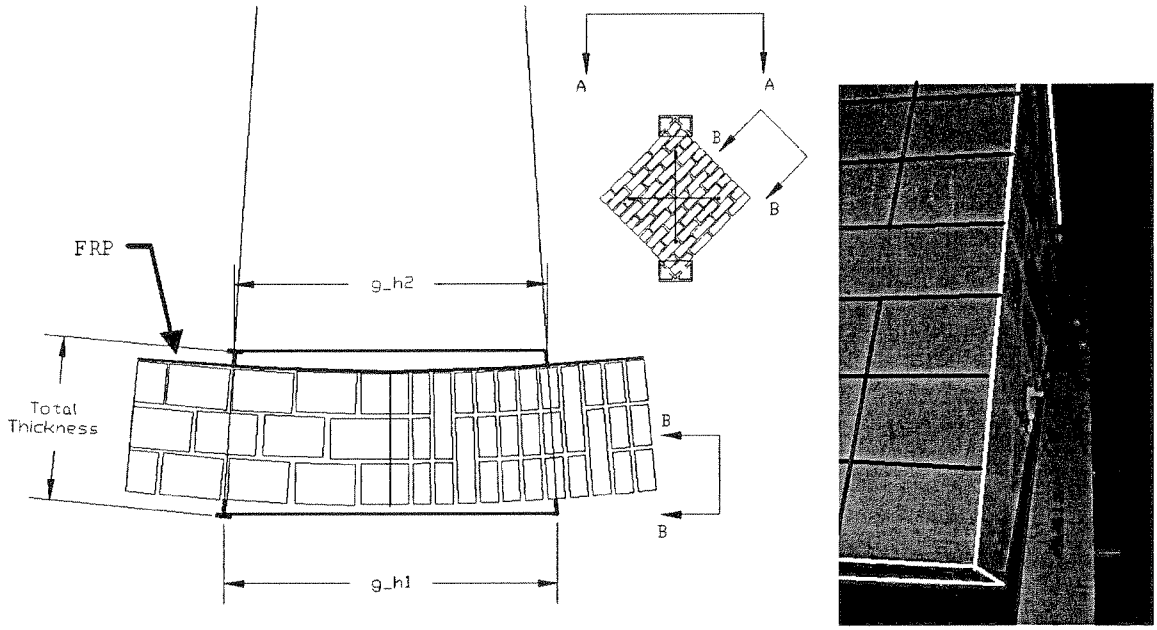

SECTION A-A SECTION B-B

Figure 21: Section A-A shows curvature about the vertical axis where curvature as drawn is negative. *g_h1* and *g_h2* are the gage lengths of the horizontal displacement transducers on side 1 and side 2, respectively. Section B-B shows a photograph of Side 1 with the panel edges and bricks outlined for clarity. Curvature is evident from the yardstick which lies horizontally across the non-FRP side of the retrofitted Wall 6. The yardstick corresponds with *g_h1* and touches the brick panel at its center, but not at the ends.

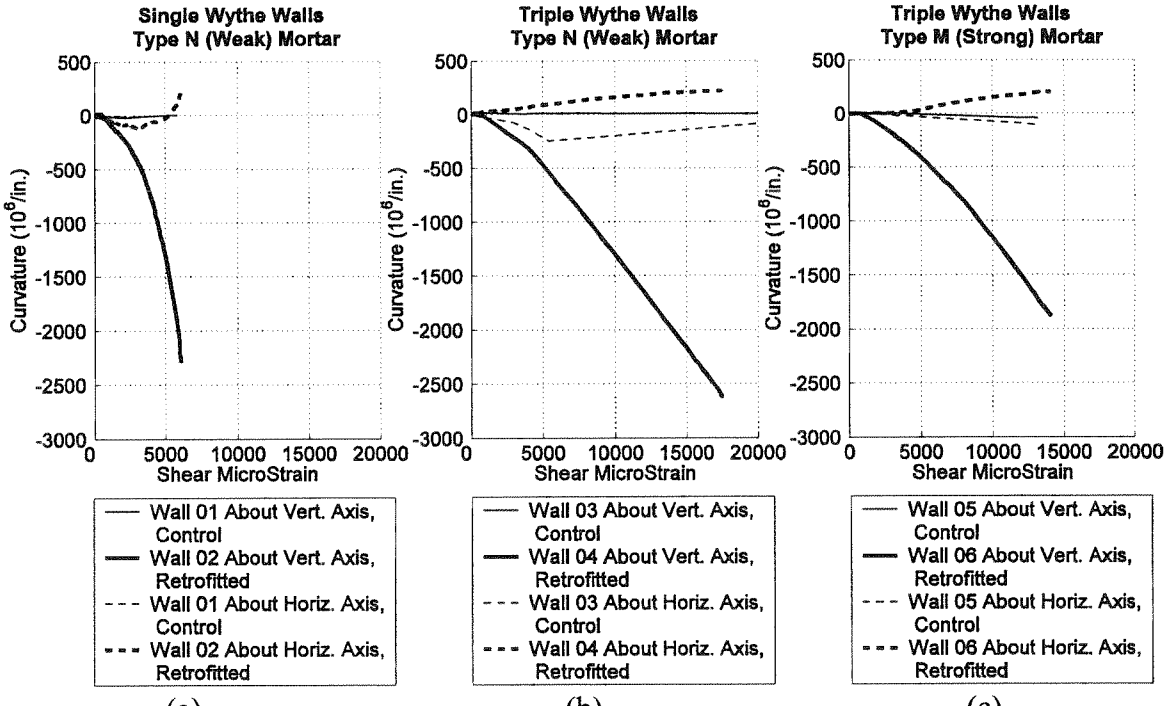

(a) (b) (c)

Figure 22: Comparison of wall curvature about the horizontal and vertical axes.

(knife-edge) load may also increase the likelihood of splitting (Mosalam, 2003).

5.4.3 Axial Loads

Axial load also has a significant effect on the performance of a URM wall. High axial loads tend to increase the bond strength between bricks and mortar, whereas low axial loads allow slipping of bricks over one another. In the test model, the compression force in the wall shown in Figure 4 (c) increases proportionally with the transverse load, increasing the bond strength between brick layers as the shear strength also increases. During an actual earthquake, compression loads are not likely to increase proportionally with lateral loads. In fact, overturning moments may cause the compression force to decrease with increasing lateral load.

5.4.4 Test Setup and Instrumentation

The non-cyclic quasi-static test method also limited the models' ability to mimic the behavior of a prototype wall during an actual earthquake. The brittle nature of URM walls makes them very vulnerable to cyclic loading where the energy input is much

Figure 23: Separation of the outer wythe in the parapet of a historic URM building. December 22, 2003 San Simeon, California earthquake (http://peer.berkeley.edu/san_simeonEQ/).

different than in a monotonic test. A retrofitting with FRP may improve cyclic response through energy dissipation mechanisms but no such energy dissipation effect could be evaluated during the non-cyclic tests. It is also important to note that the addition of FRP on only one side of the wall introduces an eccentricity in the structure. The potential negative effects of this eccentricity may only become apparent in a dynamic test of an entire building. It is thus important not to indiscriminately place FRP on various walls without considering the effect on the entire structural system response.

In addition to the limitations due to the experimental model, analysis of the tests was somewhat limited by the test machine and instrumentation. The walls were loaded using force control operated by the laboratory technician who adjusted a dial to increase and decrease the rate of loading. In the elastic range, the loading rate was relatively consistent across all specimens. However, as soon as cracking occurred, some variation in applied loads and corresponding displacements may have occurred for each specimen. Also, loading continued until it was judged that further loading would be unsafe due to complete separation and falling of the walls rather than to a specific strain value. The ultimate strain was defined as occurring when the wall strength deteriorated to 75% of the yield stress, but for many of the specimens, the wall was actually loaded to much greater strains.

Readings of the loading cell and displacement transducers were taken every second. When cracking occurred, the exact load path during cracking could not be determined, so linear approximations were made between data points as shown in the previous graphs. The displacement transducers measured to within 0.001 in. and the loading cell measured forces to within about 200 lb. This instrumentation accuracy was

sufficient to provide a reasonable understanding of how each wall performed. Moreover, since these parameters are almost identical in all specimens, comparisons between specimens are warranted.

6 Design Implications

The experiments conducted for this study focus on evaluating changes in the behavior of a masonry panel when retrofitted with FRP. The experiments sought to examine the effect of FRP on the panels as a material component rather than attempting to model the actual seismic response of a URM wall within a building. Despite this limitation of scope, it is still important to place this material enhancement within the context of retrofit design. In the United States, URM is generally evaluated according to either the Prestandard and Commentary for the Seismic Rehabilitation of Buildings (FEMA 356, 2000) or the Building Code Requirements for Masonry Structures (ACI 530-02/ASCE 5-02/TMS 402-02, 2002). Both documents offer guidance for estimating the strength of existing URM structural walls or piers. The two publications will be collectively called *the codes* throughout this chapter though technically, FEMA 356 is a "prestandard" and not a building code.

This chapter calculates the design shear strength and initial stiffness of hypothetical prototypes of the experimental walls according to these two codes. It is important to note that the design strengths are not adjusted to account for different design philosophies (e.g. allowable stress design versus strength design or linear versus nonlinear design), so a larger design shear strength does not necessarily permit design for a greater lateral load according to the codes. The permissible lateral load may depend on load factors from local building codes, reduction factors for nonlinearity, the strength of other actions in the wall (e.g. bending moment), design objectives, importance factors,

and many other possible design considerations. Because of the difficulty in equating each code's method for computing required lateral strength, only the design strengths are considered in this chapter.

After the shear strength and stiffness are calculated according to the codes, two design techniques are proposed for estimating the strength enhancement provided by retrofitting the hypothetical URM walls on one side with FRP. The estimation of FRP contribution to strength is made by consulting the *Acceptance Criteria For Concrete And Reinforced And Unreinforced Masonry Strengthening Using Fiber-Reinforced Polymer (FRP), Composite Systems* (ICBO AC125, 2001) and the *Guide for the Design and Construction of Externally Bonded FRP Systems for Strengthening Concrete Structures* reported by (ACI 440.2R-02, 2002), both of which are used as guidance for estimating the shear strength contribution. The authors also propose another method for approximating the FRP strength contribution based on shear strain. These estimates are then compared with the actual experimental results.

6.1 Comparing the Design Wall with Experimental Results

6.1.1 Prototype Wall

For the purposes of comparison, three hypothetical walls are proposed for design, each wall corresponding with one of the three control specimens tested. The prototype walls are distorted scales of the experimental panels in that the length and width are increased by a factor of four, but the thickness is unchanged. Consequently, force and displacement scale by a factor of four and strains, stress, and drift do not change. The hypothetical length, $L = 120$ *in.*; the effective height, $h_{eff} = 120$ *in.;* and the single-wythe wall thickness, $t = 3\text{-}5/8$ *in.* and the triple-wythe thicknesses, $t = 11\text{-}5/8$ *in.*. The walls are

assumed to be free-standing cantilevers subjected to a lateral force, V, distributed uniformly at the top of the wall and a gravity force (an unfactored dead load), N. The gravity force is set equal to the specimens' experimental "yield" shear force (as discussed in the next sub-section), because as shown in Figure 4 (c), the normal force equals the shear force in the experiments ($N = P_{y,exper} / \sqrt{2} = V_{y,exper}$). Though the normal force, N, is set equal to the experimental shear force, the design shear strength developed from the codes will not equal the assumed normal force. However, by keeping the normal force constant, the various design methods can be compared equitably.

6.1.2 Evaluation of Experimental Results

Various design shear strength and stiffness are calculated in the sections below. The predicted shear strength and stiffness of these hypothetical walls will then be compared with the experimental results from the panels tested in this study. The strengths of the experimental panels are expressed as the yield shear force

$$V_{y,exper} = \left(P_y / \sqrt{2}\right) S_F \tag{16}$$

where P_y is the applied force at the yield shear defined in Chapter 4 and S_F is the scale factor for force ($S_F = 4$) to scale the experimental results to the prototype wall.

The shear stiffness of the experimental panel can be defined based on either shear force and drift or the shear modulus (based on shear stress and shear strain). The two approaches do not lead to similar results because of the assumptions used to calculate drift in Equation (6). The experimental stiffness calculated from drift is defined as

$$k_{\delta,exper} = V_{y,exper} / \left(\delta_y h_{eff}\right) \tag{17}$$

where δ_y is the experimental drift at yield. The experimental stiffness calculated from the shear modulus is defined as

$$k_{\gamma,exper} = G_{exper} A_v / h_{eff} \tag{18}$$

where A_v is the shear area of the prototype wall (435 in.^{2} and 1395 in.^{2} for the single-wythe and triple-wythe walls, respectively), and G_{exper} is the shear modulus calculated from the experiments and defined as

$$G_{exper} = \tau_y / \gamma_y \tag{19}$$

where τ_y and γ_y are respectively the experimentally-determined shear stress and corresponding shear strain at yield as defined in Chapter 4.

After the scaled strength and stiffness of the control panels are compared with code predicted values, the increase in shear strength provided by the FRP, V_{FRP}, is predicted and then compared with the actual scaled change in shear strength from the experiments. The difference in strength between the control and retrofitted experimental panels are evaluated using three different criteria: yield strength, ultimate strength, and maximum strength. The difference is calculated for each of the three criteria for each of the three pairs of control and retrofitted specimens. The scaled experimental shear force resisted by the FRP in the wall is defined as

$$V_{FRP} = \left(V_{retrofit} - V_{control}\right) S_F \tag{20}$$

For the yield strength criterion the experimental shear forces, $V_{retrofit}$ and $V_{control}$, are measured at each panel's respective yield strain. Similarly for the ultimate strain criterion, the strengths are measured at each panel's respective ultimate strain in spite of that fact that the retrofit and control panels may have significantly different ultimate strains. The maximum strength criterion is based on the overall maximum shear force resisted by each

panel which, obviously takes place at a different strain values for different panels. The reasons behind evaluating the FRP shear resistance using these three criteria will be discussed later.

6.1.3 Discrepancies Between the Prototype and the Experimental Panels

It is important to note that the experimental panels were not intended to mimic exactly the stress states that would be present in an actual building during a seismic event, whereas the equations from the codes are intended to predict seismic response in a prototype structure. Assuming a cantilever boundary condition in the prototype permits axial force, overturning moment, and shear force to develop in the hypothetical walls, but the wall panels in the test setup were subjected to a stress state more similar to a pure shear loading condition. Section 7.3.3.3.3 of FEMA 356 specifically cautions against using the diagonal tension test to predict the response of prototype shear walls for the following reasons:

- Extrapolation of the test data to actual masonry walls is difficult because the ratio of shear to normal stress is fixed at a constant ratio of 1.0 for the test specimens.
- The distribution of shear and normal stresses across a bed joint may not be as uniform for a test specimen as for an actual wall.
- Any redistribution of stresses that would occur after first cracking in a prototype wall will not be well represented in the test specimens.

The section concludes that test data cannot be useful to predict nonlinear behavior. This chapter only seeks to provide some context as to how the experimental results from this study compare with current retrofit design practices. It is not expected that the predictions from the codes will correspond with the values from the experiment. Despite these

limitations, conclusions made based on the relative behavior of retrofitted and control wall panels are still valid and valuable.

6.2 FEMA 356

6.2.1 Overview

FEMA 356 contains nationally applicable provisions for the rehabilitation of buildings to improve seismic performance. The prestandard contains requirements for selecting a rehabilitation objective and conducting the seismic rehabilitation process. Guidelines are provided for choosing a linear or nonlinear analysis. A linear analysis procedure is followed for this design example. Also, based on the shape of the force-displacement curves, the prestandard requires a design based on either deformation-controlled or force-controlled actions. For deformation-controlled components, the expected strength, Q_{CE}, shall be used, where Q_{CE} is the statistical mean value of yield strengths, Q_y, for a population of similar components. Elements governed by deformation-controlled actions shall satisfy

$$m\kappa Q_{CE} \geq Q_{UD} \tag{21}$$

where m is the component or element demand modifier to account for expected ductility, κ is the knowledge factor, and Q_{UD} is the deformation-controlled design action due to gravity and earthquake loads.

For a force-controlled action, a lower bound estimate of the component strength, Q_{CL}, shall be used where Q_{CL} is the statistical mean minus one standard deviation of the yield strengths, Q_y, for a population of similar components. Elements governed by force controlled actions shall satisfy

$$\kappa Q_{CL} \geq Q_{UF} \tag{22}$$

where Q_{UF} is the force-controlled design action. For the purposes of comparison to the experiment values and ACI 530 (discussed in Section 6.3), κQ_{CL} or κQ_{CE} will be assumed to equal the design strength depending on whether force or deformation control applies. In other words, m, in Equation (21) will be moved to the right hand side of the equation as a reduction factor on Q_{UD}.

In the following two sub-sections, shear strength and stiffness will be computed using the default masonry shear strengths given in Chapter 7 of FEMA 356, the actual bed-joint shear strengths found from the material experiments, and the largest bed-joint shear strength allowed by FEMA 356. The masonry compressive strength is always defined according to the prism tests performed. From the three different masonry shear strengths and the prism test, the overall strength and stiffness of the hypothetical walls will be calculated and compared with the experimental results.

6.2.2 Shear Strength

FEMA 356 provides equations for both the expected lateral strength and the lower bound lateral strength of URM walls and piers. Section 7.4.2.3 of FEMA 356 states that URM walls and piers shall be considered deformation-controlled components if their expected lateral strength is less than the lower bound lateral strength. If the walls and piers do not meet this requirement, the walls and piers should be considered force-controlled. Failures governed by diagonal tension cracking or toe compression failure are considered brittle and are therefore required to be force-controlled based on the lower bound lateral strength. Bed-joint sliding shear and rocking are considered more ductile failure modes and consequently, deformation-controlled analysis is allowed and expected

lateral strengths should be used. In this section, first the expected lateral strength is calculated and then these values are compared with the lower bound lateral strength.

The expected lateral strength of URM walls and piers are calculated according to the lesser of the lateral strength based on expected bed-joint sliding shear strength or expected rocking strength, calculated in accordance with Equations (23) and (24), respectively

$$Q_{CE} = V_{bjs} = v_{me} A_n \tag{23}$$

$$Q_{CE} = V_r = 0.9 \alpha P_E \left(\frac{L}{h_{eff}} \right) \tag{24}$$

where v_{me} is the expected masonry shear strength, A_n is the area of the net mortared section (435 in.^{2} and 1395 in.^{2} for the single-wythe and triple-wythe wall, respectively, where throughout this chapter the core area is not subtracted because the entire section of mortar contributes to strength), α is a factor that equals 0.5 for fixed-free cantilever walls or 1.0 for fixed-fixed piers (the fixed-free condition is assumed to exist), P_E is the expected axial compressive force due to gravity loads ($P_E = 1.1N$), L is the length of the wall or pier (120 in.), and h_{eff} is the height to the resultant of the lateral force (120 in.).

For URM components of walls and piers, FEMA 356 recommends that expected masonry shear strength, v_{me}, be calculated using an approved in-place shear test. UBC 21-6 offers a standard for testing masonry shear strength, which is further described by Section C7.2.2.4 of FEMA 274. The test involves measuring the horizontal force required to move an in-situ brick. The test was not performed on the experimental walls used in this study though the direct shear tests described in Chapter 2 should produce similar data. Since Section 7.3.2.10 of FEMA 356 allows default material properties to be

used in the determination of component strengths for the linear analysis procedures in Chapter 3 of FEMA 356, the default values will be used first to evaluate their validity. The compressive strength of the masonry prisms are 2906 psi and 3472 psi for Type N and Type M mortars, respectively, so the masonry condition will be assumed to fall in the category of "Good" in Table 7-1 of FEMA 356. The "Good" condition corresponds with a default expected compressive strength of 1170 psi from Table 7-1, significantly lower than the average of the experimental tests. The default expected masonry shear strength for this condition is 35.1 psi for masonry with a running bond lay-up. Using this default strength value in Equation (23), the expected lateral strength based on the bed-joint slipping failure mode of the single-wythe and triple-wythe URM wall is 15.3 kips and 49.0 kips, respectively. The rocking strength values are much larger, and so, bed-joint slipping controls the deformation-controlled action. Since the default strength values are used, the deformation-controlled design strengths are expectedly much lower than the experimental values as shown in Table 8.

Next, the expected lateral strength used for deformation-controlled components is compared with the lower bound lateral strength used for force-controlled components. Lower bound lateral strength, Q_{CL}, shall be taken as the lesser of the diagonal tension strength and the toe compressive strength calculated using the following equations, respectively

$$Q_{CL} = V_{dt} = f'_{dt} A_n \left(\frac{L}{h_{eff}}\right)\sqrt{1+\frac{f_a}{f`_{dt}}} \tag{25}$$

$$Q_{CL} = V_{tc} = \alpha P_L \left(\frac{L}{h_{eff}}\right)\left(1-\frac{f_a}{0.7f`_m}\right) \tag{26}$$

where L / h_{eff} shall not be taken less than 0.67 for Equation (26), f'_{dt} is the lower bound masonry diagonal tension strength, f'_m is the lower bound masonry compressive strength from prism tests ($f'_m = f'_{me} / 1.6$ where f'_{me} is the expected masonry compressive strength taken from the prism test results shown in Table 7), f_a is the expected axial compressive stress ($f_a = P_E / A_n$), and P_L is the lower bound axial compressive force ($P_L = 0.9N$). FEMA 274 states that because tests do not exist for masonry diagonal tension strength, the masonry shear strength, v_{me}, as measured with the in-place shear test may be substituted for f'_{dt} where it is assumed the *lower* bound diagonal tension strength is equal to the *expected* value of the masonry shear strength. Of course, the lower bound masonry diagonal tension strength is ideally found using the exact experimental test setup used in this study. Clearly, the lower bound lateral strength, Q_{CL}, calculated from the diagonal tension strength from the experiments in this study will be much larger than the expected lateral strength, Q_{CE}, calculated in Equation (23) using the default masonry shear strength. Consequently, the suggested replacement of f'_{dt} with the default value of v_{me} will be used here, because this procedure is more typical of what would be conducted in practice where a f'_{dt} value may not be available and because the resulting lower bound lateral strength, Q_{CL}, is more justifiably compared with the expected lateral strength, Q_{CE}, calculated above.

From the values in Table 8, it is evident that the diagonal tension strength calculated by using the default masonry shear strength is greater than the expected strength based on the bed-joint sliding shear failure mode. Thus, if the default material values were correct, the specimen would be deformation-controlled according to FEMA 356, and the failure mode in a prototype wall would be bed-joint sliding. The expected

shear strength, Q_{CE}, governed by bed-joint sliding failure is then multiplied by the knowledge factor, κ, to obtain the design shear strengths of 11.5 kips and 36.7 kips for the single-wythe wall and triple-wythe walls, respectively. Here, $\kappa = 0.75$, because it is assumed that no material tests were performed. Of course, since the default masonry shear strength (35.1 psi) is drastically different from the actual material values (156 psi for the Type N mortar and 232 psi for the Type M mortar determined from the direct shear tests), the predicted prototype shear strength is about $1/8^{th}$ of the experimental value. Because of the use of the default strength values for bed-joint sliding and an experimental setup that creates an overall stress distribution that does not mimic the prototype cantilevered wall, the code predicts a failure mode that is inconsistent with the diagonal tension failure mode observed in the experiment.

Table 8: Shear strength predicted by FEMA 356 using default values

	Expected Lateral Strength, Q_{CE}		Lower Bound Lateral Strength, Q_{CL}		Lateral Design Strength κQ_{CE}	Exper. Shear Strength $V_{y,exper}$
	Based on Bed-Joint Sliding V_{bjs}	Based on Rocking V_r	Based on Diagonal Tension Stress V_{dt}	Based on Toe Comp. Stress V_{tc}		
Equation	(23)	(24)	(25)	(26)	-	(16)
Units	(kips)	(kips)	(kips)	(kips)	(kips)	(kips)
Single Wythe, Type N	15.3	43.5	41.4	32.7	11.5	88.0
Triple Wythe, Type N	49.0	154.7	102.4	127.6	36.7	312.6
Triple Wythe, Type M	49.0	210.4	107.7	174.3	36.7	425.0

A closer estimate of the experimental shear strength can be obtained using the actual shear strength of the mortar-brick interface. The direct shear test described in Chapter 2 should yield very similar results to an in-situ shear test performed in accordance with FEMA 274 as described above. Equation (7-1) in FEMA 356 states that the expected masonry shear strength can be calculated using

$$v_{me} = \frac{0.75\left(0.75v_{te} + \frac{P_{CE}}{A_n}\right)}{1.5} \tag{27}$$

where P_{CE} is the expected gravity compressive force applied to the wall, which can be taken as equal to $V_{y,exper}$. v_{te} is the average bed-joint shear strength, v_{to}, given by Equation (7-2) in FEMA 356

$$v_{to} = \frac{V_{test}}{A_b} - P_{D+L} \tag{28}$$

where V_{test} refers to the bed-joint shear test load at first movement of a masonry unit, A_b is the sum of the net mortared area of bed joints above and below the test unit, and P_{D+L} is the stress due to gravity loads at the test location, where FEMA 356 assumes the coefficient of friction is one. The shear strength, v_{to}, according to the direct shear test is 156 psi and 232 psi for the Type N and Type M mortar, respectively. FEMA 356 states that values for the bed-joint shear strength, v_{te}, in Equation (27) shall not exceed 100 psi. Also, the 0.75 factor on v_{te} shall not be applied for single-wythe masonry walls, since the factor is included to deduct the estimated shear resistance from the collar joint in a multi-wythe wall, which is the ratio of the areas of the top and bottom bed joints to the sum of the areas of the bed and collar joints for a typical clay unit. For this study, the 0.75 factor is never applied since the in-situ tests were not performed. Since the experimentally tested values are much greater than the maximum allowable value, the maximum allowable value will be used. The total shear stress is then multiplied by a reduction factor equal to 0.75 and divided by 1.5 to convert it to an average stress for use with walls of a rectangular cross section. Assuming the maximum bed-joint shear strength, $v_{to} = 100$

psi, the shear strength of the masonry, v_{me}, can be calculated from Equation (27). The corresponding values are shown in Table 9.

Table 9: Maximum shear strength permitted by FEMA 356

	Expected Masonry Shear Strength v_{me}	Expected Lateral Strength, Q_{CE}		Lower Bound Lateral Strength, Q_{CL}		Lateral Design Strength κQ_{CE}	Exper. Shear Strength $V_{y,exper}$
		Based on Bed-Joint Sliding V_{bjs}	Based on Rocking V_r	Based on Diagonal Tension Stress V_{dt}	Based on Toe Comp. Stress V_{tc}		
Equation	(27)	(23)	(24)	(25)	(26)	-	(16)
Units	(psi)	(kips)	(kips)	(kips)	(kips)	(kips)	(kips)
Single Wythe, Type N	151	65.7	43.5	103.4	32.7	32.7	88.0
Triple Wythe, Type N	150	208.6	154.7	279.2	127.6	127.6	312.6
Triple Wythe, Type M	190	264.8	210.4	346.2	174.3	174.3	425.0

By increasing the expected masonry shear strength from $v_{me} = 35.1$ *psi* in Table 8 to the reported values in the second column of Table 9, the bed-joint sliding failure mode no longer controls and instead, toe compressive failure controls the strength. Since comprehensive experimental tests would be required to obtain a value for v_{to}, the knowledge factor is assumed to be 1.0. With toe compressive failure controlling design, the experimental values are still roughly twice as large as the design strength. Note that using the actual direct shear strength values rather than 100 psi would not increase the shear capacity, since the capacity will still be governed by the toe compressive stress failure mode, which is independent of the shear strength (see Table 10).

It is interesting to note that the strength assuming a diagonal tension failure mode is greater than the experimental shear strength even when the maximum allowable bed-joint shear stress is used (Table 9). If the actual material shear strength values from the direct shear test are used (results shown in Table 10), the lower bound diagonal tension strength for the single wythe wall is 30% higher than the measured strength. Perhaps

further investigation is necessary to ensure that the code predicted strengths are sufficiently conservative.

Table 10: FEMA 356 estimated shear strength using experimental material properties

	Expected Masonry Shear Strength v_{me}	Expected Lateral Strength, Q_{CE}		Lower Bound Lateral Strength, Q_{CL}		Lateral Design Strength κQ_{CE}	Exper. Shear Strength $V_{y,exper}$
		Based on Bed-Joint Sliding V_{bjs}	Based on Rocking V_r	Based on Diagonal Tension Stress V_{dt}	Based on Toe Comp. Stress V_{tc}		
Equation	(27)	(23)	(24)	(25)	(26)	-	(16)
Units	(psi)	(kips)	(kips)	(kips)	(kips)	(kips)	(kips)
Single Wythe, Type N	179	78.0	43.5	116.8	32.7	32.7	88.0
Triple Wythe, Type N	190	265.4	154.7	338.0	127.6	127.6	312.6
Triple Wythe, Type M	268	374.5	210.4	458.8	174.3	174.3	425.0

6.2.3 Stiffness

FEMA 356 also offers methods of estimating wall stiffness. According to Section 7.3.2.7 of FEMA 356, the expected shear modulus of masonry, G_{me}, shall be permitted to be taken as 40% of the elastic modulus in compression, E_{me}. The elastic modulus in compression was not measured for these experiments, but the default value from FEMA 356 can be used. Assuming "Good" masonry condition, the expected elastic modulus in compression, E_{me}, shall be taken as $550f'_{me}$ where f'_{me} is the expected masonry compressive strength taken from the prism test results shown in Table 7.

According to Section C7.4.2.1 of FEMA 356, laboratory tests of solid shear walls have shown that conventional principles of mechanics for homogeneous materials can be used to predict the behavior of solid shear walls at low force levels. The lateral in-plane stiffness of a cantilevered shear wall, k, can be calculated as

$$k = \frac{1}{\frac{h_{eff}^{\ 3}}{3E_{me}I_g} + \frac{h_{eff}}{A_v G_{me}}} \tag{29}$$

where the shear area of the section is assumed equal to the net area, A_n, defined above and I_g is the moment of inertia for the gross section representing uncracked behavior (522×10^3 in.^{4} and 1674×10^3 in.^{4} for the single-wythe and triple-wythe specimens, respectively).

Equation (29) considers flexural deformation in the first term of the denominator and shear deformation in the second term of the denominator. Stiffness is calculated using both terms in the fourth column of Table 11. These values should be representative of the prototype wall. However, the experimental setup creates a stress distribution closer to pure shear without flexural deformation. By setting the first term in the denominator equal to zero, only the shear stiffness is calculated and this value (the fifth column of Table 11) should be more consistent with the experimentally observed stiffness.

As was briefly discussed at the beginning of this chapter, the experimental stiffness is calculated in two ways using either the shear strain, $k_{\gamma,exper}$ or the drift, $k_{\delta,exper}$, both of which are reported in Table 11. The large difference between these two methods ($k_{\gamma,exper} \approx 2k_{\delta,exper}$) reveals an overall inconsistency in the ability of the test setup to model the stiffness of an actual wall. At yield the vertical deformations measured by the displacement transducers are about four times larger than the horizontal deformations. In an ideal pure shear stress state, the magnitude of the deformations would be the same, so a state of pure shear does not actually exist in the experimental panel. In addition, the vertical deformations are spread out consistently throughout the gage length whereas the horizontal deformation is concentrated along the center of the panel with relatively little

strain near the corners. This conclusion is based on strain contours from finite element analysis of the experiments conducted by Nguyen as reported in (Nguyen, 2003). The strain contours are shown in Figure 24 and Figure 25. Both of these inconsistencies in the strain distributions show that the panel is not actually in pure shear and the calculation of a shear strain is a very rough approximation of the actual behavior. Similarly, the drift Equation (6) assumes a pure shear stress distribution and the equation only uses the vertical deformation, which explains why the stiffness based on drift is half as much as the strain-based stiffness calculation. These inconsistencies explain both why the calculation of the experimental stiffness depends largely on the method used and why neither of the experimental stiffnesses correspond closely with the code predicted stiffness with no flexural deformation. When flexural deformation is considered, the predicted stiffness values are relatively close to the drift-based experimental stiffness values, but this similarity should be interpreted as a coincidence, since the experimental tests do not permit flexural deformation.

Table 11: Comparison of FEMA 356 and experimental stiffness

	Elastic Modulus E_{me}	Shear Modulus G_{me}	Stiffness, assuming flexural deformation k	Stiffness, assuming no flexural deformation k	Exper. Stiffness $k_{\delta,exper}$	Exper. Stiffness $k_{\gamma,exper}$
Units	(ksi)	(ksi)	(kips/in.)	(kips/in.)	(kips/in.)	(kips/in.)
Equation	$550f_{me}$	$0.4E_{me}$	(29)	(29)	(17)	(18)
Single Wythe, Type N	1598	639	891	2318	733	1462
Triple Wythe, Type N	1598	639	2858	7432	2430	4836
Triple Wythe, Type M	1910	764	3415	8880	3182	4976

6.3 ACI 530-02/ASCE 5-02/TMS 402-02

The Masonry Standards Joint Committee created the Building Code Requirements for Masonry Structures to be referenced in legally adopted building codes. Unlike FEMA

356, ACI 530 is intended for new construction and not rehabilitation of existing buildings, but the code does contain provisions for URM buildings that can be used for assessment of existing buildings. ACI 530 permits URM to be designed according to Allowable Stress or Strength Design, both of which are discussed below.

6.3.1 Allowable Stress Design

The Masonry Standards Joint Committee reports a method of calculating shear strength of URM walls similar to FEMA 356. The code states that the design strength is equal to the nominal strength multiplied by a strength reduction factor ϕ, which equals 0.6 for shear. The design strength must be greater than the required strength, U. The nominal strength shall be taken as 2.5 times the allowable stress value and is permitted to be increased by one-third for load combinations including earthquakes. Thus,

$$f_v \leq \phi\left(2.5 \cdot 1.33 \cdot F_v\right) \tag{30}$$

where F_v is the allowable shear stress. The required shear stress, f_v, is equal to

$$f_v = \frac{VQ}{I_n b} \tag{31}$$

where V is the shear force applied to the wall, Q is the first moment of area about the neutral axis of a section of that portion of the cross section between the neutral axis and extreme fiber, I_n is the moment of inertia of the net cross-sectional area of a member, and b is the width of the section. ACI 530 considers three failure modes as described in the Commentary. Equations (32), (33), and (34) consider these three failure modes, namely, (1) formation of diagonal tension cracks through the mortar and masonry units, (2) sliding along a straight crack at horizontal bed joints, and (3) formation of stepped cracks

alternating from head joint to bed joint. The allowable in-plane shear stress, F_v shall not exceed any of

$$F_v \leq 1.5\sqrt{f'_m} \tag{32}$$

$$F_v \leq 120 psi \tag{33}$$

$$F_v \leq v + 0.45 N_v / A_n \tag{34}$$

where f'_m is the specified compressive strength of masonry from prism tests according to ACI 530.1/ASCE 6/TMS 602, $v = 37 psi$ for masonry in running bond that is not grouted solid, N_v is the compressive force acting normal to the shear surface, which is set equal to the experimental yield shear force, $V_{y,exper}$, A_n is defined for this section as the gross cross-sectional area of the masonry as allowed by the Commentary (435 in.^{2} and 1395 in.^{2} for the single-wythe and triple-wythe wall, respectively). f'_m is determined from the prism tests reported in Table 7. ACI 530 does not explicitly state that material tests can be used to increase the value used for v. Therefore, only the results using the default values are shown in this report. According to ACI 530 equations, diagonal shear cracking is the governing failure mode for the prototype wall. Despite this similarity in predicted failure mode, the maximum allowed shear force is about half the experimental values as shown in Table 12.

6.3.2 Strength Design

For Strength Design, the masonry wall should be proportioned such that the design shear strength, ϕV_n, shall exceed the shear corresponding to the development of 1.25 times the nominal flexural strength, M_n, except that the nominal shear strength, V_n, need not exceed 2.5 times the required shear strength, V_u. The strength reduction factor,

ϕ, shall be taken as 0.8 for masonry subjected to shear. The strength design method seems to consider the same failure modes as allowable stress design, though the failure modes are not explicitly stated. Nominal shear strength, V_n, shall be the smallest of

$$V_n \leq 3.8 A_n \sqrt{f`_m} \tag{35}$$

$$V_n \leq 300 A_n \tag{36}$$

$$V_n \leq 56 A_n + 0.45 N_v \tag{37}$$

For strength design, Equation (37) governs, which corresponds with the bed-joint sliding failure mode. The nominal and design shear strengths are shown in Table 12. The shear strength design values are lower than the experimental values, but they are reasonable considering the simplicity of the experiment, the high variability, and the different failure mode that is predicted.

Table 12: Shear strength predicted by ACI 530

	Allowable Stress Design			Strength Design		Exper. Shear Strength $V_{y,exper}$
	Allowable Shear Stress F_v	Adjusted Allowable Shear Stress	Maximum Allowed Shear Force V	Nominal Shear Strength V_n	Design Shear Strength ϕV_n	
Units	(psi)	(psi)	(kips)	(kips)	(kips)	(kips)
Equation	(32)	(30)	(31)	(35)	-	(16)
Single Wythe, Type N	80.9	161	46.8	64.0	51.2	88.0
Triple Wythe, Type N	80.9	161	150.0	218.8	175.0	312.6
Triple Wythe, Type M	88.4	176	164.0	269.3	215.5	425.0

The strength design values are slightly higher than the allowable stress design values, which is reasonable since the seismic forces in strength design would be increased by appropriate load factors. Interestingly, Equation (37), which corresponds with the bed-joint sliding failure mode now governs the response, which means that the failure mode

predicted by the code is dependent on whether an allowable stress design or a strength design approach is adopted.

6.3.3 Stiffness

Unlike FEMA 356, ACI 530 does not specify a particular equation to estimate wall stiffness. Section 1.8.2.2.1 of ACI 530 does state that the modulus of clay masonry shall be taken as $E_m = 700 f'_m$ where the masonry compressive strength is multiplied by a factor of 700 instead of 550 in FEMA 356. The shear modulus is still taken as 40% of the compressive modulus. If Equation (29) is again used to calculate the code predicted stiffness, the ACI 530 predicted stiffness will simply be 27% higher ($700 / 550 = 1.27$) than the FEMA 356 stiffness values shown in Table 11, since the stiffness is linearly proportional to the elastic modulus.

6.4 Expected FRP Contribution

The contribution of FRP to the shear resistance of the retrofitted specimen varies according to the strain in the wall. By ensuring that the bond strength between the FRP and the masonry is large enough such that debonding does not occur, it can be assumed that the strain in the FRP equals the strain in the bricks. For a particular strain value, the stress in the FRP can be calculated assuming a linear stress-strain relationship utilizing the reported FRP modulus of elasticity. This stress can be integrated over the FRP cross-sectional area to find the total shear force resisted by the FRP. Alternatively, at any given strain, the shear resistance provided by the FRP will be equal to the shear force resisted by the bricks subtracted from the total shear force.

The publications of FRP design guidelines cited below use a tension approach, which assumes a maximum allowable design tension strain in the FRP. FRP shear strength is considered the product of this strain and the tensile modulus of the FRP. The authors propose an alternative approach that uses a maximum allowable design shear strain and the shear modulus of the FRP. The latter approach is more consistent with the calculation of the stresses in the FRP according to Equation (10). Theoretically, the tension and shear approaches should give similar results.

Regardless of the approach, choosing the maximum allowable design strain value at which the FRP strength contribution is determined, greatly affects the additional shear force resistance provided by the FRP. If a small strain value is chosen (e.g. strain at initial cracking), the total strength can be easily predicted since both the FRP strength and the masonry strength at cracking can be easily determined. However, the shear force resisted by the FRP will continue to increase as cracks in the masonry open, but the forces resisted by the masonry will decrease as the masonry is damaged. Because of the difficulty in predicting the post-cracking behavior of the retrofitted masonry walls, it is difficult to predict at what strain the retrofitted wall will resist the most shear force. The strains chosen for each FRP stress calculation will be discussed below.

6.4.1 Tensile Strain Approach

At this time, building codes have not yet been published for the design of retrofitting schemes on multi-wythe URM. However, the shear strength contribution of the glass/epoxy laminate can be calculated based on the ICBO ES *Acceptance Criteria for Concrete and Reinforced Masonry Strengthening Using Fiber-reinforced Polymer (FRP) Composite System* (AC 125, 2001). In addition, ACI Committee 440 has published

a report titled, *Design and Construction of Externally Bonded FRP Systems for Strengthening Concrete Structures*, which can be applied to masonry (ACI 440.2R-02, 2002). In agreement with section 7.3.2.6.3 of the AC 125 (2001), the design shear strength enhancement, ΦV_{FRP}, is

$$\Phi V_{FRP} = \Phi \Omega l_w \sum_{i=1}^{n} \left(t_i \left(f_i \sin^2 \theta_i + f_i \cos^2 \theta_i \right) \right) \tag{38}$$

for a rectangular wall section of length, l_w (120 in.), measured parallel to the applied lateral force. The strength enhancement is provided by n bidirectional FRP laminates with the i-th laminate having thickness, t_i (0.04 in.), with fibers at an angle, $\pm\theta_i$ ($\pm 45°$), to the wall axis. The strength reduction factor, Φ, for shear can be taken as 0.8 according to the strength design section of ACI 530. The efficiency factor, $\Omega = 0.75$, applies to FRP placed on one side according to AC 125. It should be noted that AC 125 requires that the FRP be wrapped around wall section ends to a face perpendicular to the direction of the applied shear force. The FRP for this experiment was not wrapped around the ends of the panel, but since no debonding was observed, the effect of not wrapping the wall should not be significant. Also, AC 125 requires the fiber angle to be greater than or equal to 75°, though the equation is still applicable to fibers at a 45° angle as assumed in this chapter.

To determine the design shear strength for the FRP, it is necessary to calculate the design tensile stress defined as

$$f = E\varepsilon \tag{39}$$

where ϵ is the allowable design tensile strain for shear calculations and E (2270 ksi) is the longitudinal design modulus of the FRP laminate. The modulus is not reduced by an

environmental reduction factor, because ACI 440.2 states that the modulus is generally unaffected by environmental conditions.

The permissible stress of the FRP material according to AC 125 is

$$f = 0.004E \leq 0.75 f_u \tag{40}$$

This equation assumes the allowable design tensile strain, ϵ, is 0.004. f_u is the ultimate tensile strength of the FRP laminate (44.1 ksi), which is much greater than $0.004E$. AC 125 does not explain why this value is chosen, but 0.004 was probably chosen as an estimate for the ultimate strain present in masonry and concrete shear walls. For comparison, the average ultimate shear strain of the three control walls tested for this study was 0.0053 with a COV between the three control specimens of only 7.1%.

A strain of 0.004 results in a guaranteed design tensile stress of 9.08 ksi. Inserting this stress into Equation (38) results in a FRP design strength of

$$\Phi V = 0.8(0.75)(120in.)2\left[(0.04in.)\left((9.08ksi)\sin^2 45 + (9.08ksi)\cos^2 45\right)\right] = 52.3kips$$

for all three hypothetical walls. This strength is compared with the results from the experimental study in Table 13. It is difficult to make broad comparisons with the experimental results because of the large amount of variability and the small number of specimens. However, the change in strength between the control and retrofitted triple-wythe Type N mortar specimen is close to the AC 125 predicted results regardless of whether the experimental enhancement is calculated specifically at ultimate strain or based on the overall maximum shear force resisted (See Section 6.1.2. for an explanation of the three methods used to calculate the experimental enhancement provided by the FRP).

Table 13: Design FRP Strength at Ultimate Strain Versus Experimental FRP Strength

	Tensile Stress Design		Shear Stress Design		Experiment	
	Assumed Tensile Strain	FRP Shear Force	Assumed Shear Strain	FRP Shear Force	Change in Shear Strength at Ultimate Strain	Change in Maximum Shear Strength
Units	-	(kips)	-	(kips)	(kips)	(kips)
Equation	-	(38)	-	(41)	(20)	(20)
Single Wythe, Type N	0.0040	52.3	0.0053	14.3	32.8	56.6
Triple Wythe, Type N	0.0040	52.3	0.0053	14.3	58.8	45.3
Triple Wythe, Type M	0.0040	52.3	0.0053	14.3	-86.9	-144.2

The shape of the shear stress-strain plots in Figure 13 show that the triple-wythe walls do not resist much additional shear force after initial cracking. As a result, a more conservative estimation of FRP contribution to shear resistance may be obtained using the "yield" point of the control specimens defined in Chapter 4, which approximately corresponds with the initial cracking of the bricks. The tensile strain can be approximated by simply taking the "strain" from the horizontal displacement transducer, which equals 128 microstrain with a COV between the three control specimens of 35.3%. This value corresponds with tensile cracking strain data from experiments performed on clay brick masonry reported by (Lourenco et al, 1996). While this study's experimental yield strain corresponds with data from Lourenco et al, the tensile "strain" should be interpreted with caution since it is calculated over the entire gage length of 26 in. In reality, most of the tensile strain is concentrated within a small band near the center of the panel, so the local strain in this region is much higher than the average strain taken across the gage length. This inconsistency in the definition of strain is shown by the strain contours created by Nguyen (2003). Nguyen compares the experimental results from this study with the results from finite element analysis of the same diagonal shear test specimen. Figure 24

shows that the principle compression strain is relatively uniform across the diagonal height of the specimen, while Figure 25 shows that the principle tension strain is concentrated along the load path with relatively small strain near the corners of the panel.[4] Because of this nonuniformity in strain, using the horizontal yield strain of 128 microstrain results in an especially conservative estimate of the stress in the FRP at yield (291 psi). Inserting this stress into Equation (38) results in a FRP design shear force of only 1.7 kips, about 30 times less than the code recommended value. Table 14 compares this value with the experimental change in yield shear force when the control wall is retrofitted. Again, it is difficult to make any broad comparisons, because of the inconsistency in experimental behavior, as discussed previously.

Table 14: Design FRP Strength at Yield Strain Versus Experimental FRP Strength

	Tensile Stress Design		Shear Stress Design		Experiment	
	Assumed Tensile Strain	FRP Shear Force	Assumed Shear Strain	FRP Shear Force	Change in "Yield" Shear Strength	Change in Maximum Shear Strength
Units	-	(kips)	-	(kips)	(kips)	(kips)
Equation	-	(38)	-	(41)	(20)	(20)
Single Wythe, Type N	0.000128	1.7	0.00660	1.8	11.3	56.6
Triple Wythe, Type N	0.000128	1.7	0.00660	1.8	40.9	45.3
Triple Wythe, Type M	0.000128	1.7	0.00660	1.8	-166.3	-144.2

[4] Figure 24 and Figure 25 should only be used to observe the relative strain distribution in the panels. The particular magnitudes of strains shown have no significance in the present discussion. Refer to (Nguyen, 2003) for more information regarding the finite element analysis used to create these strain contours.

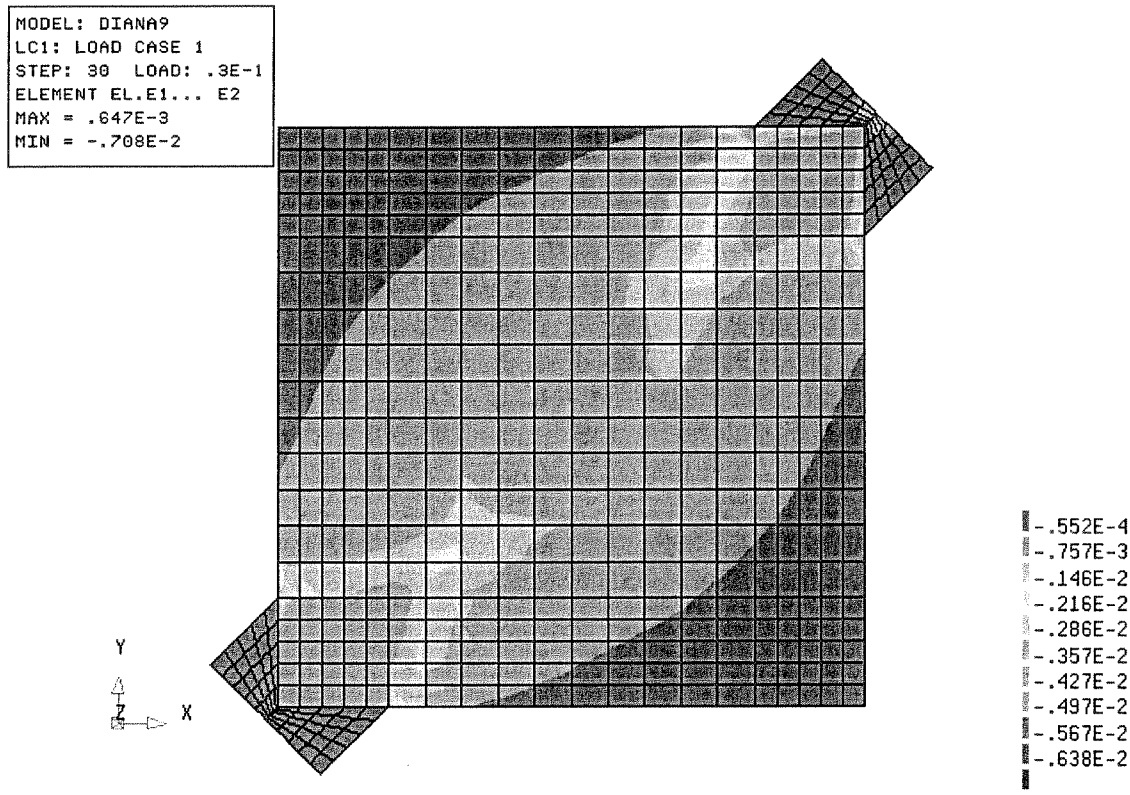

Figure 24: Principal compression strain in homogeneous system (Nguyen, 2003).

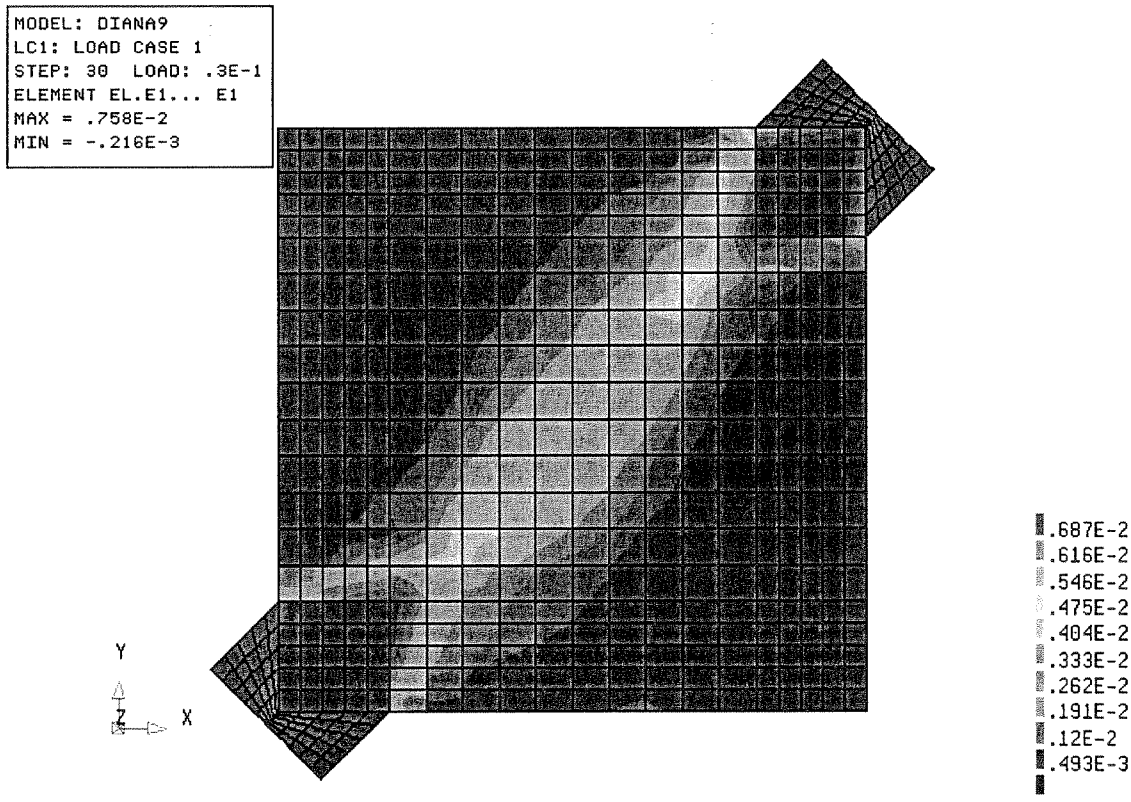

Figure 25: Principal tension strain in homogeneous system (Nguyen, 2003).

6.4.2 Shear Strain Approach

An alternative approach to estimating FRP shear strength contribution from tensile strain and the FRP tension modulus is to use shear strain and the FRP shear modulus. This shear strain approach is more consistent with estimation of the FRP shear stress in Equation (10). Using this approach, the design shear strength of the FRP is

$$\Phi V = \Phi \Omega l_w \sum_{i=1}^{n} (t_i \tau_i) \tag{41}$$

where for the i-th laminate, τ_i is the shear stress in the FRP defined as

$$\tau = G\gamma \tag{42}$$

where γ is the maximum allowable design shear strain and G is the reported shear modulus of the FRP (470 ksi). The equation only applies to laminates with bidirectional fibers oriented perpendicular to each other. It is also important that the experimentally determined laminate shear modulus is consistent with the orientation of the fibers relative to the wall as was the case for this study.

As discussed with the tensile strain approach, the maximum allowable design shear strain can be defined according to the yield shear strain or the ultimate shear strain. The average ultimate shear strain of the control specimens is 0.0053 with a COV of 7.1%, a value relatively close to the 0.004 tensile strain value recommended by the AC 125 (2001). This shear strain creates a shear stress of 2491 psi in the FRP, which results in a design shear strength of 14.3 kips for all three hypothetical walls. From Table 13, it is evident that this approach results in a calculated FRP design shear strength enhancement that is about one quarter of the design shear strength predicted by the AC 125 tensile strain approach. The large difference between the two approaches is due to the different strain values used for each approach (i.e. the tensile strain of 0.004 does not necessarily

correspond with a shear strain of 0.0053). Again, it is difficult to make any broad conclusions as to which approach better predicts the strength enhancement provided by the FRP because of the variability in experimental data.

The shear force resisted by the FRP should also be evaluated at the yield shear strain, defined as the average yield shear strain of the three experimental control specimens. The yield shear strain is 0.00066 with a COV of 9.9%, which induces a shear stress in the FRP of 310 psi. Substituting into Equation (41) results in a design shear force of 1.8 kips, which is about the same as the shear force contribution of the FRP calculated using tensile strain. At yield strain, the shear strain approach and tensile strain approach produce very similar estimates of the FRP design shear strength, because both effective strain values come from measurements on the experimental specimen. When the FRP design shear strength is calculated at the yield strain, the addition of the FRP has a minimal effect on overall strength. The experimental results from specimens with Type N mortar seem to indicate that calculating FRP shear strength enhancement at the yield strain is too conservative. However, more studies are required to validate this statement.

6.5 Design Summary

This chapter utilized FEMA 356 and ACI 530 to determine the design shear strength of a hypothetical 10 ft. x 10 ft. freestanding URM shear wall. The design strengths were then compared with the measured shear forces resisted by the experimental panels. The left column of Figure 26 shows four of the considered design strengths superimposed on the experimental drift-shear force relationship for each of the three control specimens. The code plots include the predicted stiffness of the hypothetical wall including flexure and shear contributions. Due to scaling effects, the experimental

shear force is assumed to be simply four times the actual measured shear force from the experiments.

After the code shear strength and stiffness were calculated, the FRP contribution to shear strength was predicted. The right column of Figure 26 shows the design shear strength of the URM walls retrofitted with FRP superimposed on the experimental drift-shear force relationship. The lines in the figure represent only the design strength. The stiffness is not shown. The FRP contribution is shown here using the AC 125 recommendations (labeled 5 and 7) and using the experimentally calculated yield shear strain, 0.00066 (labeled 6 and 8). These predicted FRP contributions are then added to the FEMA 356 and ACI 530 Strength Design calculations for the unretrofitted URM wall (shown in the left column) to obtain the overall design strength of a retrofitted prototype. The maximum allowed masonry stress (100 psi) is used for the FEMA 356 calculations.

It is difficult to make conclusive remarks regarding the accuracy of the design methods evaluated in this chapter, because of the variability in test results, the small number of specimens tested, and the inability of the diagonal tension test to model real URM wall behavior. The design techniques for evaluating the shear strength of a URM wall are well established, but more research is necessary to better estimate an appropriate method for predicting the additional shear strength provided by retrofitting a multi-wythe URM wall with FRP on only one side.

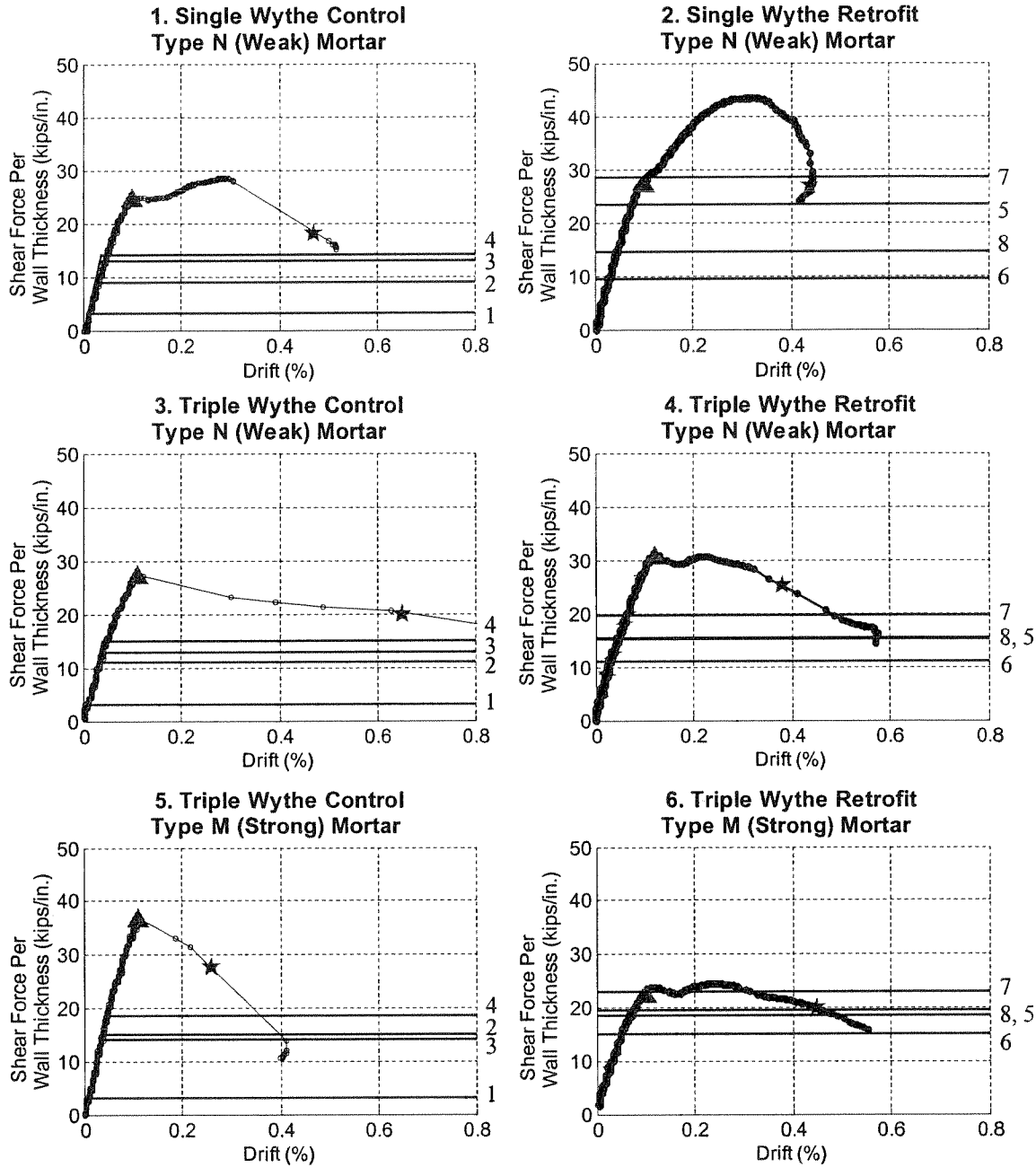

1. FEMA 356, Default Masonry Shear Strength	5. FEMA 356, Max. Allowed Stress & FRP from AC 125 with $\epsilon = 0.004$
2. FEMA 356, Max. Allowed Stress	6. FEMA 356, Max. Allowed Stress & FRP from Yield Shear Strain
3. ACI 530, Allowable Stress Design	7. ACI 530, Strength Design & FRP from AC 125 with $\epsilon = 0.004$
4. ACI 530, Strength Design	8. ACI 530, Strength Design & FRP from Yield Shear Strain

Figure 26: Predicted behavior versus experimental results for hypothetical walls.

7 CONCLUSIONS

The present investigation has shown the effect of retrofitting one side of a URM wall with ±45 degree glass fiber reinforced laminate. Two experimental objectives were studied. First, a comparison was made between the improvements in performance provided by retrofitting a single-wythe wall versus that provided by retrofitting a triple-wythe wall. Second, the performance enhancement provided by the FRP was compared with two mortar-to-brick strength ratios. Conclusions from the six walls tested using a diagonal tension (shear) configuration can be summarized as follows:

1. FRP increased the strength of the single-wythe URM wall by about 50% but had minimal effect on ductility.
2. The three-wythe wall results did not consistently show an increase in ductility or strength provided by the FRP.
3. Walls retrofitted with FRP exhibited less catastrophic failures. Upon initial cracking, the strength capacity of the retrofitted walls deteriorated at much lower strain rates than the unretrofitted walls. However, it is difficult to directly apply this result to the retrofit design of a URM building unless further in-depth investigation to develop design guidelines is performed.
4. The strong Type M mortar most likely increased the URM wall's sensitivity to flaws. Though historic URM buildings are more likely to have weak mortar relative to brick strength, testing the strong mortar showed that the addition of FRP may decrease the such sensitivity to flaws by increasing the ductility

capacity of the wall. Thus, retrofitting a historic structure with FRP may reduce a building's sensitivity to flaws caused by poor construction practices or deterioration over time. The strength of the retrofitted wall with Type M mortar was 66% of the unretrofitted wall's strength, yet the ductility was nearly two times greater.

5. Application of FRP to one side of the wall induced significant curvatures, which may significantly affect the overall seismic response of a URM building.
6. Current design guidelines provide reasonable estimates of the shear strength of a URM wall. More research is necessary to evaluate current practices for predicting the additional shear strength provided by retrofitting a multi-wythe URM wall with FRP on only one side.

The above conclusions should be considered in the limited context of the experiments conducted. Further research is needed to determine more definitively the potential advantages and disadvantages of using FRP on only one side of a multi-wythe URM wall. This future research may include the following investigations:

1. The effect of retrofitting historic URM buildings with FRP should be evaluated with consideration given to the high degree of variability in material properties and uncertainty in existing conditions. By increasing the sample size, more definitive comparisons can be made between retrofitted and unretrofitted specimens, and these comparisons can then lead to retrofit design guidelines.
2. The effect of more realistic diaphragm-wall connections with varying degrees of eccentric and concentrated loading should be considered. This investigation may reveal a tendency for wythes to split apart, which would negate any apparent

advantages provided by the application of FRP to only one side unless some type of through-thickness anchorage is provided.

3. Experiments with full-scale walls should be conducted where the effect of FRP induced curvature can be evaluated. Full-scale tests may reveal that FRP increases the likelihood of wythes splitting apart, out-of-plane failures, or overall eccentric building response.
4. Racking load tests should be conducted with varying axial loads, so that the effect of gravity loads and overturning moments can be evaluated.
5. Cyclic loading tests should be conducted, because they may reveal advantages to the proposed retrofitting scheme that were not evident in monotonic tests, particularly related to energy dissipation which is dependent on the loading history.
6. An alternative retrofitting technique should be investigated, which involves placing the FRP on only one side of the wall and then tying all wythes together with an anchor. This alternative may allow the FRP laminate to activate all the wythes in the wall and reduce a pernicious response caused by wall curvature and wythe splitting.

REFERENCES

American Concrete Institute (ACI) Committee 440 F, 2003, *Guidelines for Seismic Design of FRP Strengthening*, Subcommittee Task Force on Seismic Strengthening using FRP Composites, November 2003 Draft.

American Concrete Institute (ACI) Committee 440.2R, 2002, *Guide for the Design and Construction of Externally Bonded FRP Systems for Strengthening Concrete Structures*, ACI Committee 440, Revised October 26, 2001.

American Society of Civil Engineers (ASCE), 2000, *Prestandard and Commentary For the Seismic Rehabilitation of Buildings*, FEMA 356, Federal Emergency Management Agency, Washington DC, November 2000.

ASTM C 39, 2001, Standard Test Method for Compressive Strength of Cylindrical Concrete Specimens *American Society for Testing Materials*, Pennsylvania.

ASTM C 62, 2001, Standard Specification for Building Brick (Solid Masonry Units Made From Clay or Shale), *American Society for Testing Materials*, Pennsylvania.

ASTM C 67, 1999, Standard Test Methods for Sampling and Testing Brick and Structural Clay Tile, *American Society for Testing Materials*, Pennsylvania.

ASTM C 216, 2001, Standard Specification for Facing Brick (Solid Masonry Units Made from Clay or Shale), *American Society for Testing Materials*, Pennsylvania.

ASTM C 270, 2001, Standard Specification for Mortar for Unit Masonry, *American Society for Testing Materials*, Pennsylvania.

ASTM C 496, 1996, Standard Test Method for Splitting Tensile Strength of Cylindrical Concrete Specimens, *American Society for Testing Materials*, Pennsylvania.

ASTM C 1006, 2001, Standard Test Method for Splitting Tensile Strength of Masonry Units, *American Society for Testing Materials*, Pennsylvania.

ASTM D 3039, 2000, Standard Test Method for Tensile Properties of Polymer Matrix Composite Materials, *American Society for Testing Materials*, Pennsylvania.

ASTM D 3518, 2001, Standard Test Method for In-Plane Response of Polymer Matrix Composite Materials by Tensile Test of a ±45° Laminate, *American Society for Testing Materials*, Pennsylvania.

ASTM E 519, 1988, Standard Test Method for Diagonal Tension (Shear) in Masonry Assemblages, *American Society for Testing Materials*, Pennsylvania.

ASTM C 1314, 1991, Standard Test Method For Compressive Strength of Masonry Prisms, *American Society for Testing Materials*, Pennsylvania.

Boyton, Robert, S., 1964, Bond of Mortar to Masonry Units: Factors Influencing Strength, Extent, and Durability of Bond, *Masonry Mortar Technical Notes*, No. 3, National Lime Association, Washington, D.C., September 1964.

Drysdale, Robert G., Hamid, Ahmad A. and Baker, Lawrie R., 1994, Masonry Structures: Behavior and Design, Prentice Hall, Englewood Cliffs, New Jersey.

ICBO Evaluation Service, Inc., 2001, *Acceptance Criteria for Concrete and Reinforced and Unreinforced Masonry Strengthening Using Fiber-Reinforced Polymer (FRP), Composite Systems*, AC 125, Whittier, California.

Nguyen, H.-N., 2003, *A Study on the Mechanical Behavior and Modeling of Masonry*, Master of Engineering Report, Department of Civil and Environmental Engineering, University of California, Berkeley, Spring 2003.

Kehoe, B. E., 1996, Performance Of Retrofitted Unreinforced Masonry Buildings, *Proceedings of the Eleventh World Conference on Earthquake Engineering*, Disc 3, Paper No. 1417.

Lourenco, P. B., 1996, Computational Strategies for Masonry Structures, Delft University Press, The Netherlands.

Lourenco, Paulo B., Rots, Jan G., and Blaauwendraad, Johan, 1998, Continuum Model for Masonry: Parameter Estimation and Validation, *Journal of Structural Engineering*, Vol. 124, No. 6, June, 1998, pp. 642-652, June 1998.

Masonry Standards Joint Committee, 2002, *Building Code Requirements for Masonry Structures*, ACI 530-02/ASCE 5-02/TMS 402-02.

Mosalam, K.M., Mahin, S.A., and Rojansky, M., 2003, Evaluation of the Seismic Performance and Retrofit of Lightweight Reinforced Concrete Shear Walls, *ACI Structural Journal*, Vol. 100, No. 6, pp. 1-11.

National Information Service for Earthquake Engineering (NISEE), Earthquake Image Information System (EQIIS) and Karl Steinbrugge Image Database, http://nisee.berkeley.edu/eqiis.html.

Pacific Earthquake Engineering Research Center, M6.5 San Simeon Earthquake Reconnaissance Photo Gallery, http://peer.berkeley.edu/san_simeonEQ/ .

Petit, P.H., 1969, A Simplified Method Of Determining The Inplane Shear Stress-Strain Response Of Unidirectional Composites, *Composite Materials: Testing and Design, ASTM STP 460*, American Society for Testing and Materials, pp. 83-93.

Sathish, V., Ramamurthy, K., and Ambalavanan, R., 2000, Behavior of Masonry Mortars–A Factorial Design Approach, *The Masonry Society Journal*, Vol. 18, No. 2, pp. 23-30.

Tsang, Caroline, 2003, *Mortar Joint Mesh Reinforcement in Masonry Structures*, Preliminary Exam Report, University of California, Berkeley, Department of Civil and Environmental Engineering.

Tumialan, Jaime Gustavo, 2001, Strengthening of Masonry Structures With FRP Composites, *Ph.D. Dissertation*, Department of Civil, Engineering University of Missouri-Rolla.

APPENDIX

Details of the loading shoes are shown in Figure 27.

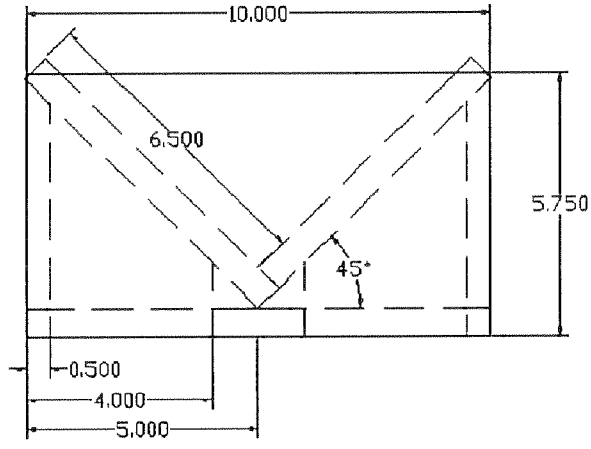

End View

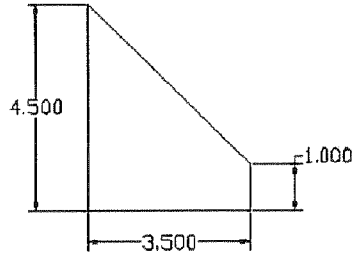

Stiffener

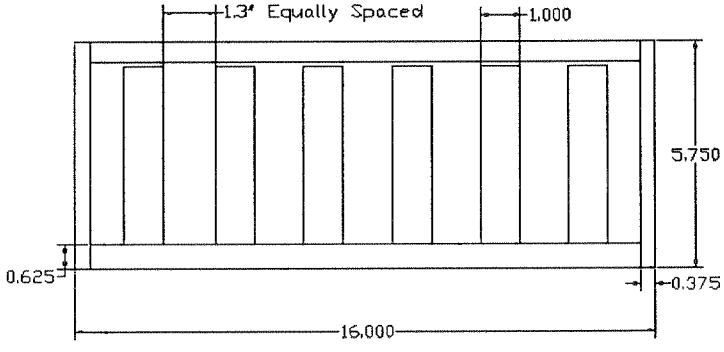

Front view: Three Wythes

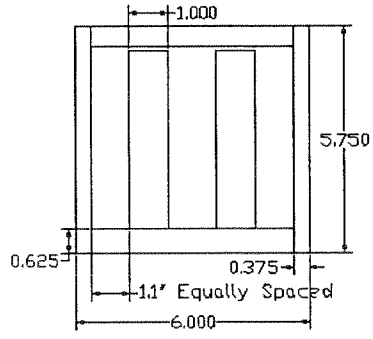

Front view: One Wythe

Figure 27: Loading shoe design.